Article

Design, Synthesis, Investigation, and Biological Activity Assessments of (4-Substituted-Phenyl)-*N*-(3-morpholinopropyl)-3-phenylthiazol-2(3*H*)-imine Derivatives as Antifungal Agents

Sazan Haji Ali, Derya Osmaniye,* Begüm Nurpelin Sağlık, Serkan Levent, Yusuf Özkay, and Zafer Asım Kaplancıklı

Cite This: *ACS Omega* 2024, 9, 39326−39343

Read Online

ACCESS | Metrics & More | Article Recommendations | Supporting Information

ABSTRACT: In this study, a series of novel thiazol-2(3*H*)-imine (**2a**−**2j**) were designed, synthesized, and characterized by means of ^{1}H NMR, ^{13}C NMR, and HRMS spectral analyses. In vitro antifungal activity was performed using a modified EUCAST protocol. Two of the synthesized compounds (**2d** and **2e**) showed activity against *Candida albicans* and *Candida parapsilosis*. Compound **2e** showed activity against *C. parapsilosis* (MIC$_{50}$ = 1.23 μg/mL) for 48 h. This value is very similar to ketoconazole. The dynamic analysis of the potential compounds **2d** and **2e** revealed notable stability while interacting with the 14α-demethylase enzyme substrate. The absorption, distribution, metabolism, and excretion (ADME) studies of the candidate compound showed acceptable ADME parameter data and verified their drug-likeness characteristics. According to the results of this study, compound 4-(4-fluorophenyl)-*N*-(3-morpholinopropyl)-3-phenylthiazol-2(3*H*)-imine (**2e**) and its derivatives as 14α-demethylase inhibitors can be used as a new antifungal for further structural improvements and additional research.

In vitro antifungal activities

Ergosterole inhibition
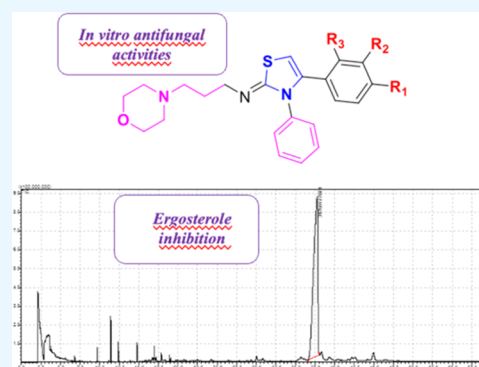
1. INTRODUCTION

The World Health Organization (WHO) released a report in 2022 that included a fungal priority pathogens list (FPPL) comprising 19 fungi that are the greatest threats to public health.[1] In doing so, the WHO attempted to systematically prioritize fungal pathogens while taking into account the unmet needs in research and development (R&D) and the perceived significance to public health. Their project's objective was to boost research efforts and examine global acceptance in order to lower the prevalence of fungal diseases and antifungal resistance.[1]

Annually, over a billion people globally suffer from fungal infections, and 1.5 million deaths among infected patients are reported.[2−4] The risk of mortality from fungal infections has considerably increased in recent years.[5] Invasive fungal infections are typically more common in patients with immunosuppressed illnesses or those who have major underlying immune system-related problems, and the risk of mortality from fungal infections has considerably increased in recent years.[5−9]

The incidence and geographic spread of fungal infections have grown recently due to global warming and improved international communications. The reported incidence of invasive fungal infections among hospitalized patients increased considerably during the COVID-19 pandemic.[10] Along with the resistance of fungi that cause typical infections like candida oral and vaginal thrush, the risks for the development of more invasive types of diseases in the general population are increasing.[1,11] The Centers for Disease Control and Prevention has estimated that the five *Candida* species comprising *Candida albicans*, *Candida glabrata*, *Candida parapsilosis*, *Candida tropicalis*, and *Candida krusei* are responsible for up to 95% of all invasive *Candida* infections in the USA.[12] Nearly two-thirds of candidemia cases in the USA are caused by non-*C. albicans* species.[8,13]

Currently, single-target medications used for the prevention and treatment of fungal infections are categorized and described based on their structural properties as follows: azoles (fluconazole, miconazole, albaconazole, etc.), polyenes (amphotericin B, nystatin), acrylamines (butenafine, naftifine, terbinafine, etc.), and antimetabolites (5-fluorocytosine).[2,14,15]
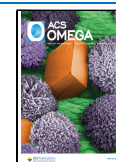
In order to overcome challenges like drug resistance, drug−drug interactions, and significant side effects that are present in currently available antifungal pharmaceuticals, it is imperative to develop new antifungal agents with high potency and safety profiles.[15−17]
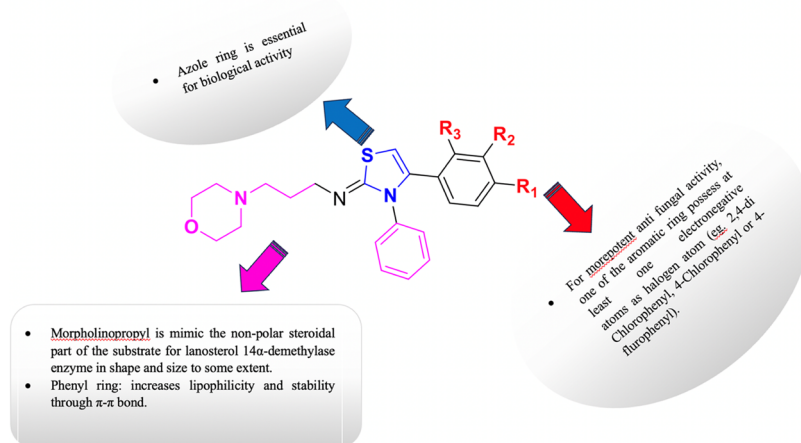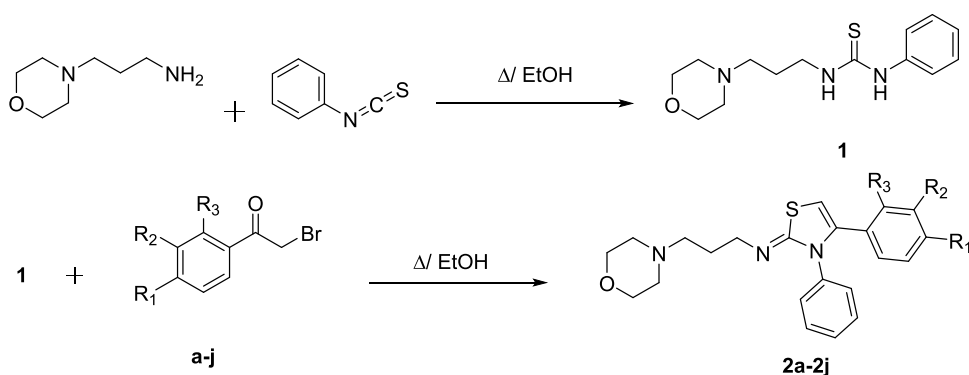
Figure 1. Structure–activity relationship of the designed compounds.

Scheme 1. General Procedure of the Synthesis of Targeted Compounds

A popular scaffold for antifungal medicines is azole heterocyclic with other heteroatoms, such as nitrogen and sulfur atoms. Azoles are a group of antifungal medications that are founded on a pharmacophore that blocks the activity of the fungus' lanosterol 14α-demethylase (also known as Erg11p, Cyp51p, and Erg16p), cytochrome P45014DM.[18] Antifungal azoles hinder the demethylation of lanosterol to ergosterol and influence the structure and function of the fungal membrane by engaging with nitrogen atoms to iron atoms of the heme group in the target protein. This restricts the synthesis of ergosterol in the fungal membrane.[18–20] Among these, antifungal medications benzimidazole and triazole are more significant and intriguing. Fluconazole, itraconazole, and voriconazole are antifungal medications that can be used therapeutically and include 1,2,4-triazole fragments. Carbendazole, benomyl, and thiabendazole are benzimidazoles that have been widely used.[2,21–24]

The fascinating class of compounds known as thiazole heterocycles has a wide range of biological activity, including antifungal characteristics.[25] A new series of [4-(4′-substituted-phenyl)thiazol-2-yl]hydrazine derivatives were synthesized by Chimenti et al.[26] The compounds were assayed for their in vitro broad-spectrum antifungal activity, compared to those of clotrimazole and fluconazole, against 20 clinical isolates of pathogenic *Candida* spp. The results showed that the presence of a heterocyclic thiazole ring revealed a promising selective inhibitory activity especially against *C. albicans* and *C. glabrata*.[26]

A decision was made to synthesize a series of new thiazole ring derivatives to evaluate their antifungal activity against *Candida* species after being inspired by other earlier studies to show the effectiveness of the thiazole ring as an antifungal agent (Figure 1).

2. RESULTS AND DISCUSSION

2.1. Chemistry. The outline synthesis of target derivatives **2a**−**2j** is given in Scheme 1. First, 3-morpholinopropan-1-aminium was refluxed with phenyl isothiocyanate to obtain compound (**1**). The precipitate (**1**) was dried and refluxed with a series of 2-bromoacetophenone derivatives in ethanol for about 6 h. After the reaction was cooled, the precipitate of a series of derivatives was filtered and obtained purely (Table 1). The structures of the synthesized compounds were elucidated by ^{1}H NMR, ^{13}C NMR, and mass spectroscopy data. The 3-morpholinopropan-1-aminium group in all compounds was observed as broad and multiplet peaks in the range of 1−4 ppm. The peaks of thiazole methine (−CH) protons, which are a common peak in all of the compounds, were observed as singlets in the range of 6.08−6.90 ppm. The signals belonging to aromatic protons were found at 6.90−7.95 ppm. The ^{13}C NMR spectra of all compounds were examined, all spectra were counterpart to the number of carbon atoms in each compound. The most characteristic peaks are of dihydrothiazole C-5 ranges at 93.37−99.23. The **2D** NMR of compound **2i** was also assessed to confirm the synthesis of the designed molecules (Table 2). All mass spectra were in accordance with the estimated M+H/1 values (Supporting Data).

Table 1. Chemical Structure of the Synthesized Derivatives (2a−2j)

comp.	R_1	R_2	R_3
2a	−CH$_3$	−H	−H
2b	−NO$_2$	−H	−H
2c	−OCH$_3$	−H	−H
2d	−Cl	−H	−H
2e	−F	−H	−H
2f	−CN	−H	−H
2g	-phenyl	−H	−H
2h	−Cl	−H	−Cl
2i	−F	−H	−F
2j	−CH$_3$	−H	−CH$_3$

Table 2. 2D ^{1}H NMR and ^{13}C NMR Analyses of 2i Compound
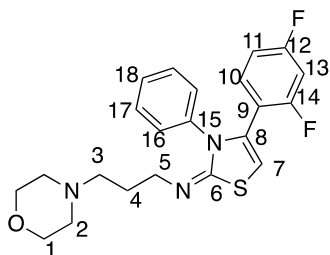
#	^{1}H value (ppm)	^{13}C value (ppm)
1	3.80	63.6
2	2.97	53.7
3	3.70	42.5
4	2.01	22.3
5	3.11	51.2
6		158.6
7	6.36	99.2
8		132.3
9		115.4
10	7.68	134.2
11	7.26	112.9
12		163.7
13	7.49	105.3
14		160.4
15		151.8
16	7.05	121.6
17	7.34	130.0
18	7.03	123.4

There are two different closing possibilities in the formation of the thiazole ring (Figure 2). To understand which of these

Prediction 1   **Prediction 2**
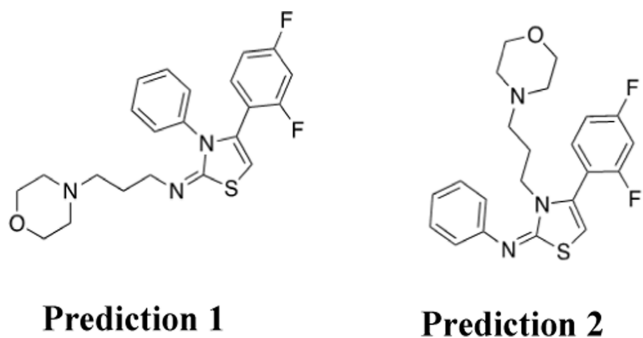
Figure 2. Prediction of the thiazole ring closure of compound **2i**.

possibilities given above was closed, 2D NMR analyses were performed, and it was determined which one it was with NOESY. If it were obtained as prediction 2, an interaction between the hydrogens on the aliphatic chain and the hydrogens on the difluorophenyl would be expected. Similarly, no interaction is expected with aliphatic hydrogens and hydrogen in the thiazole ring. However, when the correlation spectrum is examined, there is no interaction between aliphatic hydrogens and difluorophenyl, and there is a clear interaction with thiazole hydrogen. If we assume that it is closed as prediction 1, an interaction is expected between the aliphatic chain, monosubstituted phenyl, and thiazole hydrogen, and no interaction is expected with difluorophenyl. Since all expected conditions were met, it was accepted that the ring was closed as in the first case and the compounds obtained were obtained in this way (see Supporting Data).

2.2. In Vitro Antifungal Activity against *Candida* Strains. The obtained compounds, **2a−2j**, were evaluated for antifungal activity against *C. albicans* (ATCC 24433), *C. parapsilosis* (ATCC 22019), *C. krusei* (ATCC 6258), and *C. glabrata* (ATCC 90030) according to the protocol of the European Committee on Antimicrobial Susceptibility Testing.[27]

In accordance with the activity studies, compounds **2d** and **2e** were determined to be more effective derivatives, based on their IC$_{50}$, values against the *C. albicans* strains (4.75−2.37 μM/24 h), and the values indicated better effectiveness during a 48 h assessment (2.47−2.37 μM/48 h). Compared to the standard substances, compounds **2d** and **2e** showed better antifungal activity against *C. parapsilosis*, with IC$_{50}$ values of 2.37−2.47 μM/24 h and 2.37−1.23 μM/48 h, respectively (Table 3). Additionally, compounds **2g** and **2i** exhibited an MIC$_{50}$ value of 2.15−2.36 μM during a 48 h assessment against *C. parapsilosis*. The most effective derivative in the series was determined to be compound **2e**, which showed higher antifungal activity against *C. albicans* and *C. parapsilosis* species, comparable to those of fluconazole and ketoconazole.

The antifungal activity results clearly indicated that variable groups at the para position of the phenyl moiety had an essential impact on the biological activity. It was observed that the presence of stronger electronegativity, i.e., fluoride (F 4.0) and chloride (Cl 3.16) atoms, such as in compounds **2d** and **2e**, significantly enhanced antifungal activity when compared with compounds that carry lower electronegative atoms at the para position on the phenyl moiety.[28] Augmented electron density may be a reason for better antifungal activity due to the presence of electronegative atoms on the aromatic rings in compounds **2d** and **2e**. It is known that lipophilicity is a key property that influences the ability of a drug to reach the target by transmembrane diffusion and show effective biological activity. The quantitative structure−activity relationship (SAR) determined that compounds **2d** and **2e** have enough lipophilic character to show similar activity as reference substances.[29] Therefore, it might be inferred that the higher lipophilic and/or electronic characteristics of compounds **2d** and **2e** contributed to their greater antifungal activity.[18]

In general, elevated molecular lipophilicity frequently follows the development of biologic potency. However, high lipophilicity can have unfavorable absorption, distribution, metabolism, and excretion (ADME) characteristics and toxicity, which obstruct the development of new drugs. As a result, molecular lipophilicity is currently thought to be a key determinant of a drug candidate's quality.[30] On the basis of

Table 3. MIC$_{50}$ (μM) Values of Compounds 2a−2j

	24 h				48 h			
compounds	*C. albicans*	*C. parapsilosis*	*C. krusei*	*C. glabrata*	*C. albicans*	*C. parapsilosis*	*C. krusei*	*C. glabrata*
2a	628.14	39.67	628.14	>1000	317.26	19.85	317.26	628.14
2b	9.22	18.42	>1000	>1000	**4.62**	9.22	589.62	>1000
2c	9.55	38.22	611.25	305.62	9.55	9.55	305.62	305.62
2d	**4.75**	**2.37**	75.67	151.33	**2.37**	**2.37**	75.67	75.67
2e	**2.47**	**2.47**	39.37	78.71	**2.47**	**1.23**	19.70	19.70
2f	9.68	77.35	>1000	309.41	9.68	19.36	309.41	309.41
2g	549.45	**4.31**	137.36	549.45	274.73	**2.15**	68.68	137.36
2h	17.49	34.97	>1000	>1000	8.75	8.75	279.64	139.82
2i	37.66	**4.72**	301.20	>1000	18.84	**2.36**	150.60	602.41
2j	153.56	**4.81**	>1000	>1000	76.78	**4.81**	614.25	>1000
ketoconazole	1.85	1.85	1.85	3.69	0.92	1.85	1.85	1.85
fluconazole	3.20	3.20	6.40	6.40	3.20	3.20	3.20	6.40
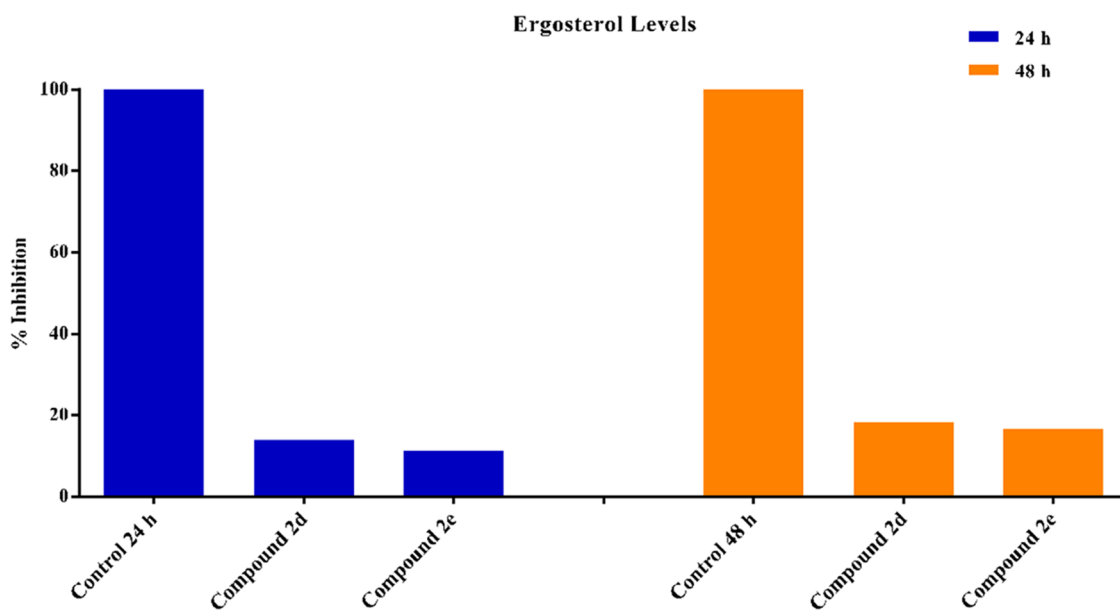
Figure 3. % ergosterol levels of compounds **2d** and **2e** on *C. parapsilosis*.

this rationale, it was thought that para fluoro substituted molecule **2e** had more potency (Table 3) than **2d**, even though it had a lower log P than **2d**, as shown in Table 5 (see below).

2.3. Ergosterol Inhibition Analysis by GC-MS. The primary sterol in yeast is ergosterol, which is crucial for maintaining the structure and functionality of cell membranes.[31] The azole antifungal medication targeted CYP51, which was encoded by the fungus' ERG11 gene. By preventing the formation of ergosterol and accumulating harmful sterol intermediates, the azole ring showed antifungal effects.[32,33] Gas chromatography−mass spectrometry (GC-MS) was used to assess the effects of compounds **2d** and **2e** on the sterol content of the cell membranes of *C. parapsilosis*. The assay was performed by applying compounds **2d** and **2e**, at their MIC$_{50}$ concentrations (24 and 48 h), to the *C. parapsilosis* cell membrane. The GC-MS chromatograms of this assay are listed in Figures 4 and 5. Considering the data obtained from these chromatograms, the effective levels of the related compounds on ergosterol at 24 and 48 h, according to the growth control groups (without any inhibitor), were calculated, and the graphic in Figure 3 was obtained. According to the observed ergosterol levels, compound **2d** inhibited ergosterol synthesis at rates of 86.055 and 81.813%, respectively, for 24 and 48 h.

As for compound **2e**, the ergosterol content was reduced at rates of 88.638 and 83.373%, respectively, for 24 and 48 h. These findings showed that compounds **2d** and **2e** significantly inhibited the fungal ergosterol synthesis by inhibiting CYP51, a pathway that is comparable to the action of the azole drug action (Figures 4 and 5).

2.4. Cytotoxicity Analysis. The cytotoxicity analysis of the obtained derivatives was performed against NIH/3T3 cell lines. From the evaluated IC$_{50}$ values of the synthesized compounds, as shown in Table 4, against the pointed-out cell line, it is clear that compound (**2d-2e**) is the most precious derivative with IC$_{50}$ (148.26, 187.66 μM) against NIH/3T3 cell line, respectively. It can be concluded that both **2d** and **2e** compounds act on fungus cells with minimum probability of influencing normal cells at their effective concentrations.

2.5. Pharmacokinetic Studies (ADME Predictions) of the Targeted Compounds 2a-2j. Using SwissADME[34] and ChemDraw 17.0[35] software, the pharmacokinetic parameters ADME of the synthesized compounds **2a−2j** were evaluated. All compounds had greater Log P values than those of the ketoconazole and fluconazole reference molecules. Despite having higher log P values, **2d** and **2e** have similar activity to the reference molecules discussed above (Table 3). All of the
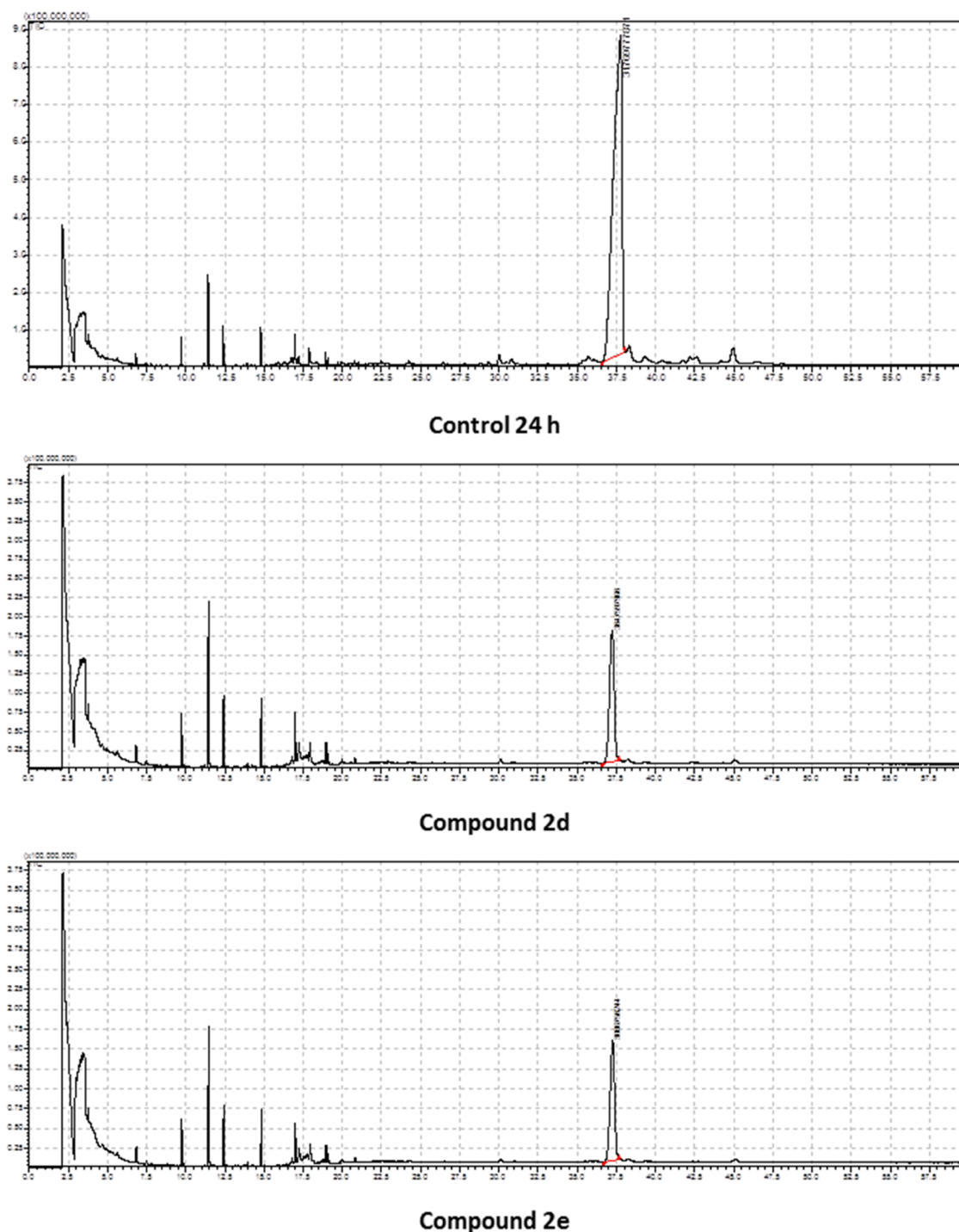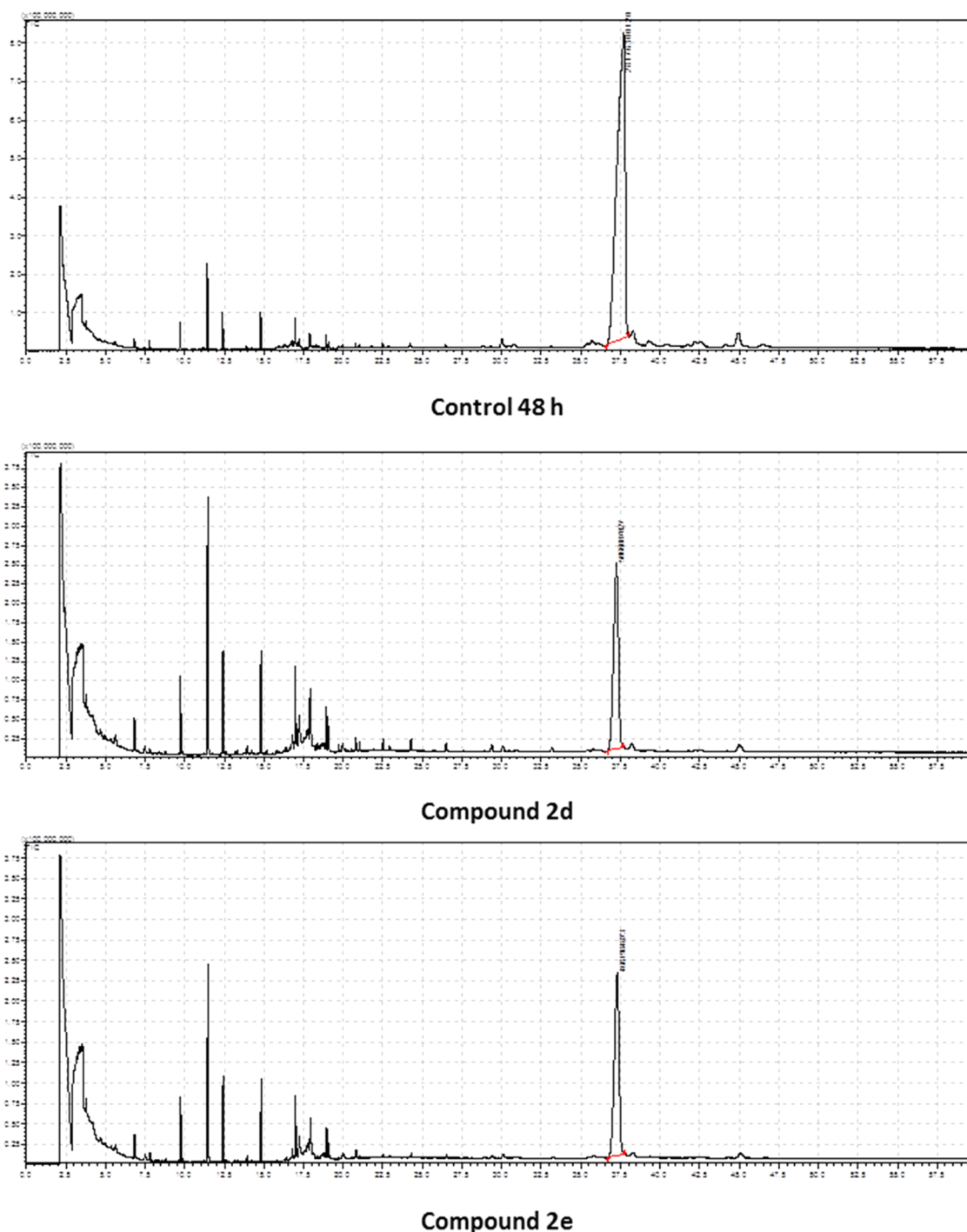
Figure 4. GC-MS chromatograms obtained from the analysis of ergosterol inhibition assay for 24 h of compounds **2d** and **2e** on *C. parapsilosis*.

compounds **2a−2j** have a high lipid solubility, which contributes to their high GI absorption. Additionally, they are Pgp substrates, which might account for their 55% bioavailability. According to the ABS, which measures compliance or noncompliance with Lipinski's rule of five, a chemical is predicted to have >10% bioavailability (F) in rats at biological pH only if it passes Lipinski's rule of five with ABS 0.55 (55% likelihood that F > 10% in rats).[36] As can be shown in Table 5, targeted compounds **2d** and **2e** exhibit sufficient ADME properties to be candidates for more assessment and research.

2.6. In Silico Studies Harmonized with Antifungal Activity. Fluconazole and a series of *N*-(3-morpholinopropyl)-3-phenylthiazol-2(3*H*)-imine derivatives (Table 1) were docked into the catalytic site of CYP51 (PDB: 1EA1)[37] using a knowledge-based approach. Fluconazole bonded to the active site of CYP51 via a coordination link with the iron of the heme group and many nonbonded contacts involving a cluster of hydrophobic residues (Tyr76 and Phe78), as shown in Figure 6.

The docking score, glide score, and glide energy of compounds **2a−2j** are presented in Table 6. According to

Figure 5. GC-MS chromatograms obtained from the analysis of ergosterol inhibition assay for 48 h of compounds **2d** and **2e** on *C. parapsilosis*.

Table 4. IC$_{50}$ (μM) Values of Synthesized Compounds (2d–2e)

compounds	NIH/3T3 (μM)
2d	148.26
2e	187.66
dox.	>1000

the molecular docking study (Figures 7 and 8), compounds **2e** and **2d** fit into the active pocket of the 14α-demethylase enzyme. The synthesized active compounds interacted

significantly with Tyr76, Phe255, Met433, Ile323, Arg96, and HEM460 residues.

Tyr76 interacted with the phenyl moiety, which is directly connected to the N atom of the thiazole ring through π−π stacking. The thiazole ring bonded to the HEM460 of the enzyme, bonded to cytochrome-p450 through π-cation interaction, to prevent oxidation of the steroidal substrate by the enzyme, and this demonstrated how crucial that moiety is.[38] Phe255, also through π−π stacking, made a connection with the thiazole moiety that increased the stability of the ligand−substrate complex.

Table 5. ADME Predictions of the Synthesized Compounds 2a−2j

| molecule	2a	2b	2c	2d	2e	2f	2g	2h	2i	2j	ketoconazole	fluconazole
log P:	5.34	3.07	4.73	5.41	5.01	4.89	6.53	4.6	5.17	5.83	3.54	0.99
C log P:	7.133	6.377	6.553	7.347	6.777	6.067	8.522	6.082	6.920	7.332	3.635	−0.44
M log P	3.2	2.84	2.64	3.47	3.36	2.3	4.01	2.31	3.74	3.41	2.47	1.47
log S:	−6.148	−6.186	−5.854	−6.487	−6.067	−5.877	−7.864	−5.911	−6.336	−6.51	−6.421	−2.127
pK_a:	7.835	7.833	7.837	7.835	7.836	7.831	7.834	7.838	7.836	7.835		11.65
GI absorption	high	high	high	high	high	high	high	high	high	high	high	high
BBB permeant	yes	no	yes	yes	yes	No	yes	yes	yes	yes	yes	no
Pgp substrate	yes	no	yes	yes	yes	yes	yes	yes	yes	yes	no	yes
CYP3A4 inhibitor	yes	yes	yes	yes	yes	yes	yes	yes	yes	yes	nes	no
log Kp (cm/s)	−5.76	−6.33	−6.14	−5.7	−5.98	−6.29	−5.25	−6.35	−6.02	−5.59	−6.46	−7.92
bioavailability score	0.55	0.55	0.55	0.55	0.55	0.55	0.55	0.55	0.55	0.55	0.55	0.55
synthetic accessibility	3.63	3.64	3.62	3.5	3.55	3.61	3.91	3.9	3.63	3.82	4.45	2.45
tPSA:	28.07	79.88	37.3	28.07	28.07	51.86	28.07	46.53	28.07	28.07	66.84	76.15
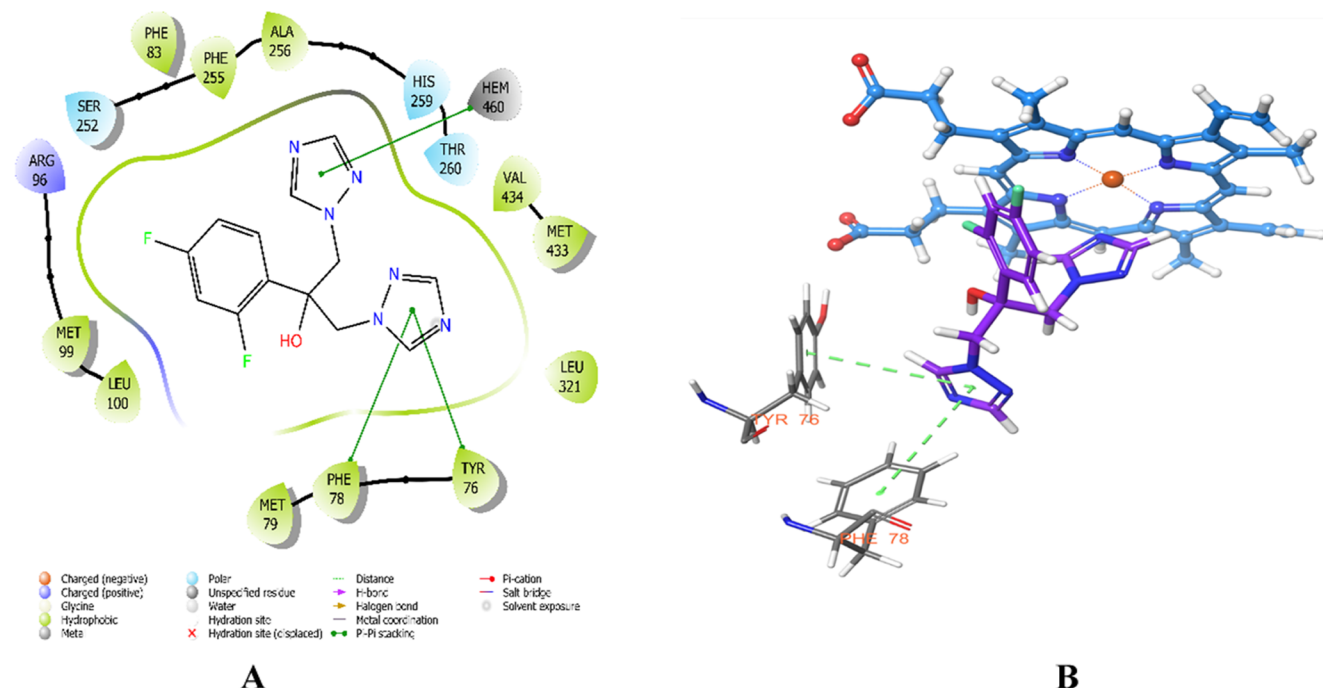
Figure 6. (A) 2D interaction mode of Fluconazole in the active region of 14α-sterol demethylase (PDB: 1EA1). (B) Three-dimensional interaction mode of Fluconazole in the active region of 14α-sterol demethylase (PDB: 1EA1).

Table 6. Docking Score (kcal/mol), Glide Score (kcal/mol), and Glide Energy (kcal/mol) of Compounds 2a−2j

| compounds	docking score	glide score	glide energy
2a	−7.636	−8.044	−36.464
2b	−7.448	−7.881	−28.163
2c	−6.960	−7.369	−23.425
2d	−8.468	−8.885	−41.399
2e	−8.023	−8.437	−36.873
2f	−6.051	−6.522	−18.083
2g			
2h			
2i	−7.339	−7.753	−31.986
2j	−7.165	−7.632	−32.022

Both Met433 and Ile323 made an H-bond with the morpholine moiety, which might have increased the interaction's strength and stability.

Figure 8 represents the molecular docking study of compound **2d**, where an additional halogen bonding interaction is present, which was missed in the 4-fluorophenyl substituted molecule **2e**. Halogen bonding between 4-chlorophenyl **2d** and the Arg96 residues demonstrated additional stiffness, which may have altered the antifungal activity. Although this bond is more necessary for ligand enzyme complex stabilization because it is stronger and resists molecule conformational changes better than H-bonds, compound **2d** demonstrated a less effective antifungal action than compound **2e**.

Moreover, the locations of the 4-chloro (**2d**) and 4-fluoro (**2e**) derivatives at the active site pockets of the enzyme were very similar, except the interaction of Cl in compound **2d** with the N of the Arg96 amino acid, in which this halogen-bond interaction was lacking in compound **2e**. One of the possible explanations for this variety is most probably related to the volume differences of the chlorine and fluorine moieties, and the other is due to the lipophilic character of the chlorine atom.[39] As a result, the in silico study explained the possible
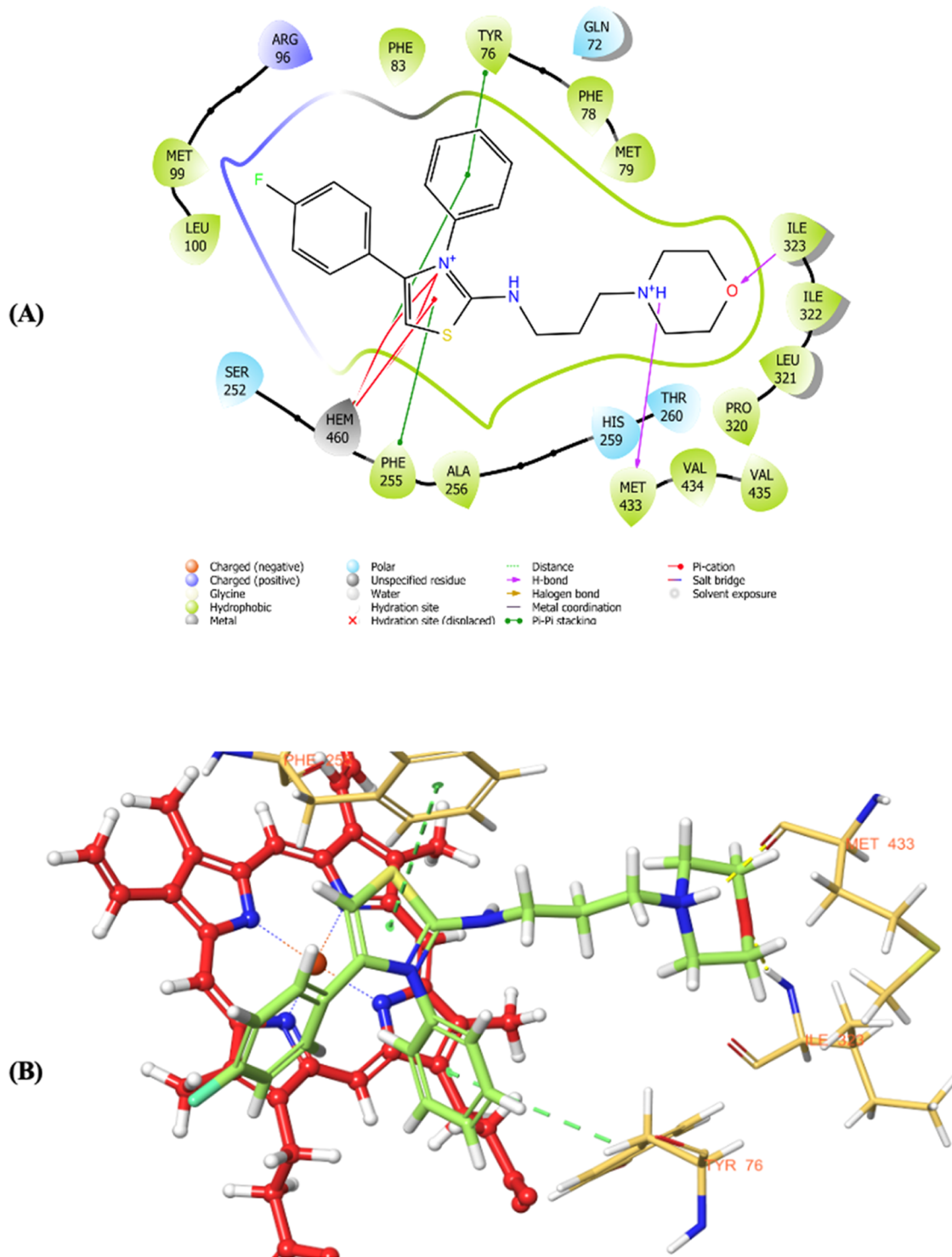
Figure 7. (A) 2D interaction mode of compound **2e** in the active region of 14α-sterol demethylase (PDB: 1EA1). (B) Three-dimensional interaction mode of compound **2e** in the active region of 14α-sterol demethylase (PDB: 1EA1). The inhibitor is colored green, and HEM red.

interaction mechanism and the SAR of the designed derivatives that fit the active binding sites of the 14α-demethylase enzyme.

2.7. Molecular Dynamics Simulations (MDS). MDS was used in this study to assess the stability of the protein−ligand complexes of selected compounds, and the results were compared with benchmark molecules. Root-mean-square deviation (RMSD), root-mean-square fluctuation (RMSF), radius of gyration (ROG), and interaction fraction were used to investigate the stability of the protein−ligand complexes.

MDS studies were used to observe and investigate the binding mechanism between the 14-demethylase enzyme and selected derivative ligands. The MDS was observed for both the **2d**-14-demethylase and **2e**-14-demethylase complexes to better understand the effect of environmental changes on the protein−ligand binding complex and characterize the SAR (Figures 9 and 11) more precisely.

The stability was examined using the guidelines below: (1) The RMSD value of the protein is calculated between 1 and 3
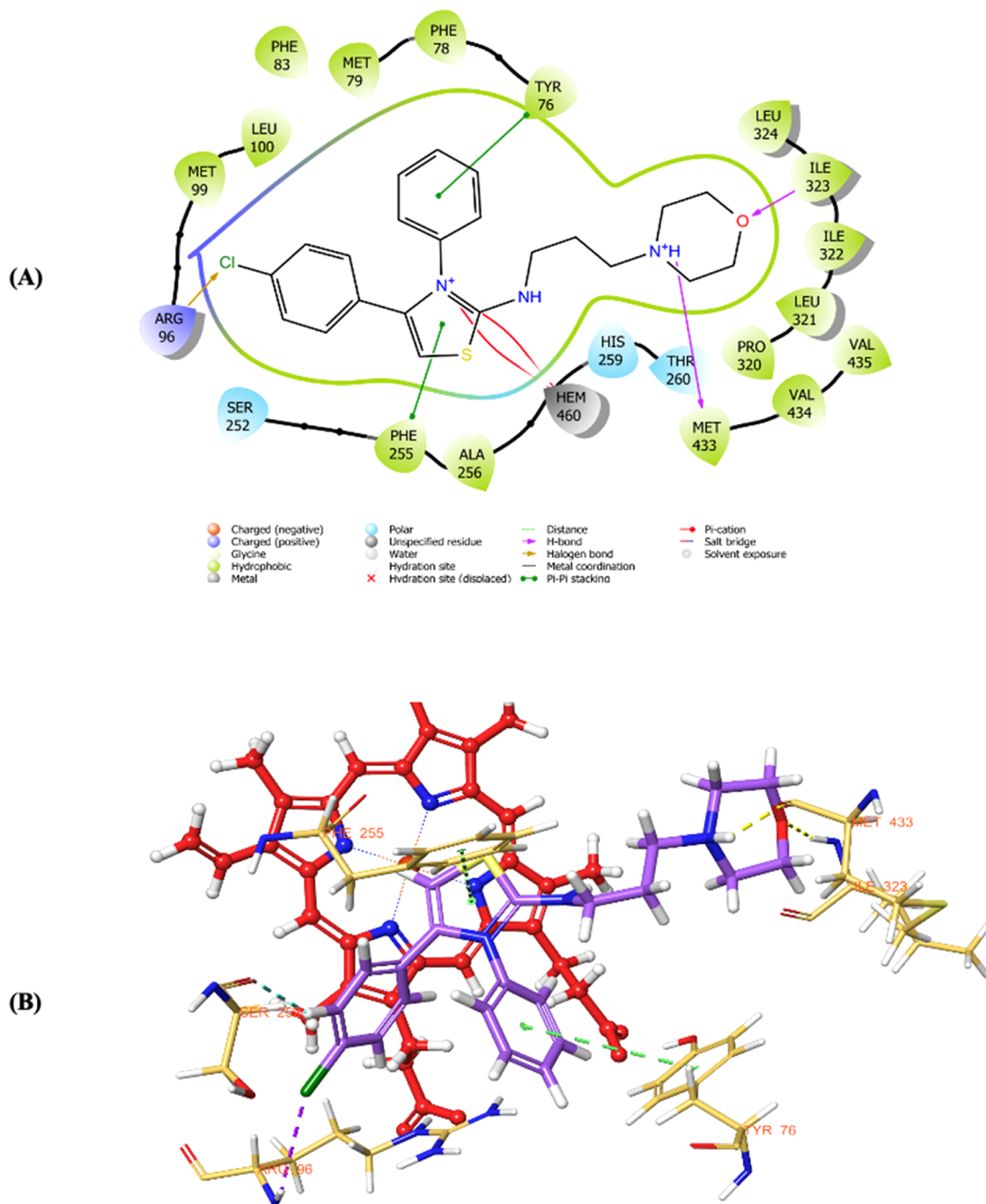
Figure 8. (A) Two-dimensional interaction of **2d** with 14α-sterol demethylase (PDB: 1EA1). (B) Three-dimensional interaction of **2d** with 14α-sterol demethylase (PDB: 1EA1), the inhibitor colored with purple, and the HEM colored with red.

Å during the entire simulation, which is indicative of stability for small proteins.[40] (2). In the ROG and RMSF plots, the picks should have minimum fluctuation. (3) The loop (white area) region may show a big fluctuation. In the MDS of **3d**, the stability properties displayed that the system was not stable until 40 ns (the equilibration phase), and after that, the system stability was reached. Moreover, there was no fluctuation within the helix, and only one of the loop regions was detected with minimal fluctuation (Figure 9).

To analyze the dynamics of the protein, the backbone RMSD from the initial structure was calculated by taking the 100 ns trajectories of each system. The binding mechanism between 14α-demethylase enzyme and **2d** molecule complex

was observed and investigated, as illustrated in Figure 9. Meanwhile, on account of the starting structure along the simulation time, the RMSD values of the protein backbone were also calculated and plotted, by checking the dynamic stability of the protein−ligand complex.

As seen in Figure 10B, the ligand **2d** and 14α-demethylase enzyme maintained uninterrupted interactions throughout the simulation. There were only minor disruptions during the 100 ns simulation due to the hydrophobic connection between the phenyl moiety and Phe83 residue. The second efficient contact involves the morpholine N atom with Tyr76 and Met433 residue. This discovery demonstrated both the stability of the
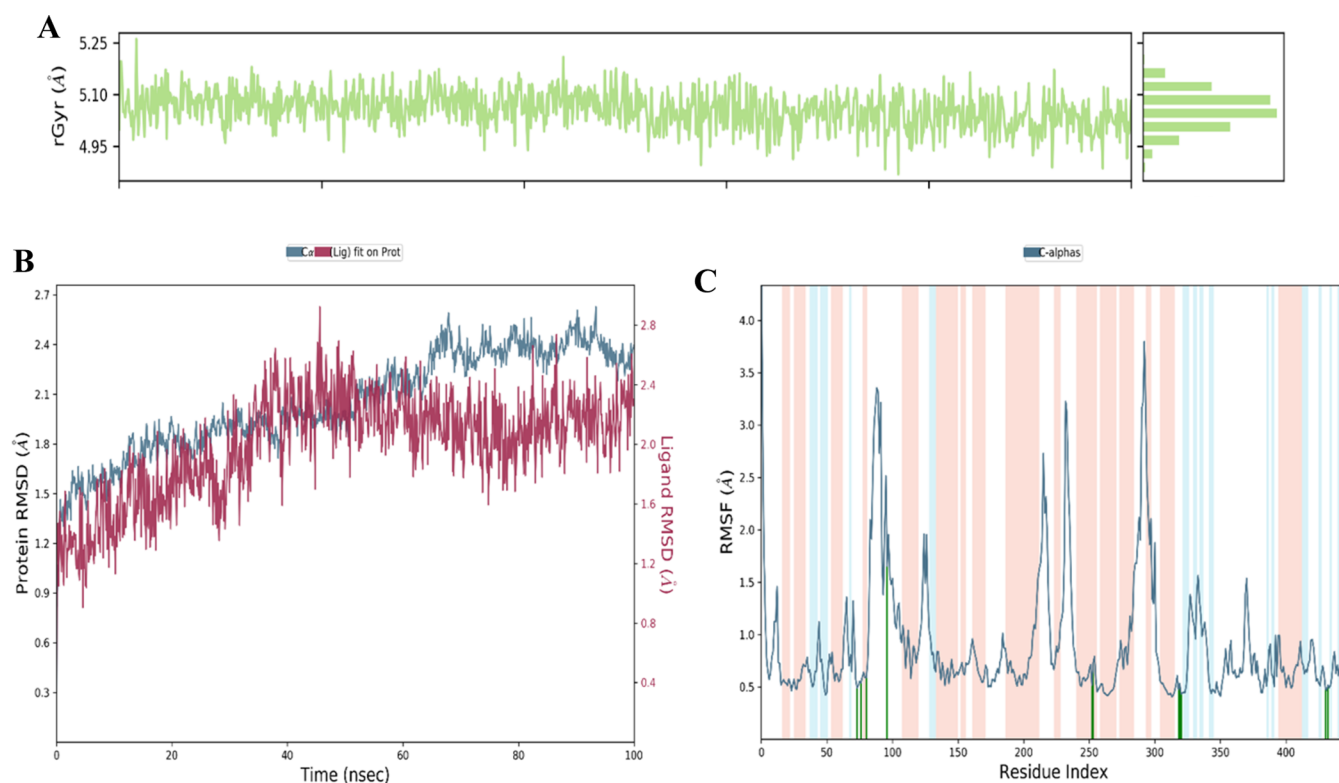
Figure 9. Stability diagrams of the compound **2d**-14α-demethylase enzyme complex. (A) Plot of radius of gyration vs time (ns), (B) plot of RMSD vs time ° (ns). (C) Plot of RMSF vs residue index (The areas were represented in light pink for the helices, light blue for the strands, and white for the loops).

ligand−protein complex and the antifungal activity, as shown in the docking study in Figure 8.

The optimal time for the ligand−protein complex to remain stable was between 40 and 60 ns. This result could be attributed to the ligand's additional, interrupted binding to Ile322 and Phe83. Another crucial link was made through Phe255, where there was only sporadic disruption between the ligand and enzyme complex during the whole simulation. All of the residues might have a significant effect on stability. Additionally, 40 ns could be seen as a turning point for the stability. Additionally, the Met433 amino acid was found as one of the important residues for antifungal activity as a 14α-demethylase inhibitor, as seen in Figure 10. Furthermore, the Tyr76 residue was also discovered to be an essential residue for assessing the activity and selectivity of 14α-demethylase inhibitors, which was found to be compatible with the literature. The overall deviations of all of the systems were within the acceptable limit (2−3 Å), as shown in Figure 10B.

The RMSF plot represents the fluctuation of each residue of a protein structure throughout the simulation. In the RMSF plot, there was not much fluctuation seen in the binding site residues in the protein−ligand complexes of the **2d** molecules (Figure 9C) when compared to the RMSF of the benchmark molecule (Figure 13C). The radius of gyration (rGyr) was calculated to measure the compactness of the protein during simulation, which suggests the stability of protein−ligand complexes. For all of the systems, the fluctuation in the rGyr values was within 1−2 Å (Figure 9A).

When the MDS results of the **2e**−14α-demethylase complex were analyzed, the presence of extra bonds was observed with different amino acid residues that were absent in the **2d**−14α-demethylase complex, as depicted in Figure 11. Cysteine 394 is

among the amino acid residues of the 14α-demethylase enzyme that established a connection with the **2e** molecule after 50 ns, and this interaction persisted intermittently throughout the remaining 100 ns, as illustrated in Figure 11B. Tyr76 consistently maintained its interaction with the **2e** molecule throughout the entire simulation, similar to what was observed in the case of **2d**. Cys394, Pro320, Arg326, and Leu321 may all play a significant role in the stability of the **2e** over **2d** molecule (Figures 11 and 12), and this distinctness may even have had an impact on their biological activities (Table 3, see above).

Making a comparison in the results of the MDS shown above of **2e** and **2d** with fluconazole, it obviously shows that in the initial 40 ns, the stability of the protein in the complex with fluconazole (benchmark compound) was observed to be more than the protein in the complex with **2d** and **2e** (Figures 9B, 11B, and 13B). During the 40 to 60 ns, complexes **2d** and **2e** showed almost the same stability. In the last 40 ns, the protein−ligand complexes of **2e** was more stable than fluconazole and **2d**. The overall deviations of all of the systems were in the acceptable limit (2−3 Å). The RMSD plot shows that compound **2d** had a more similar pattern to the benchmark compound fluconazole. In the RMSF plot, a major fluctuation was seen near the N terminal of the protein, which was away from the domain part and composed of two helices that were connected by a small loop (Figures 14). There was not much fluctuation seen in the binding site residues in the protein−ligand complexes of the benchmark or the selected molecules, **2d** and **2e** (Figures 9C, 11C, and 13C).
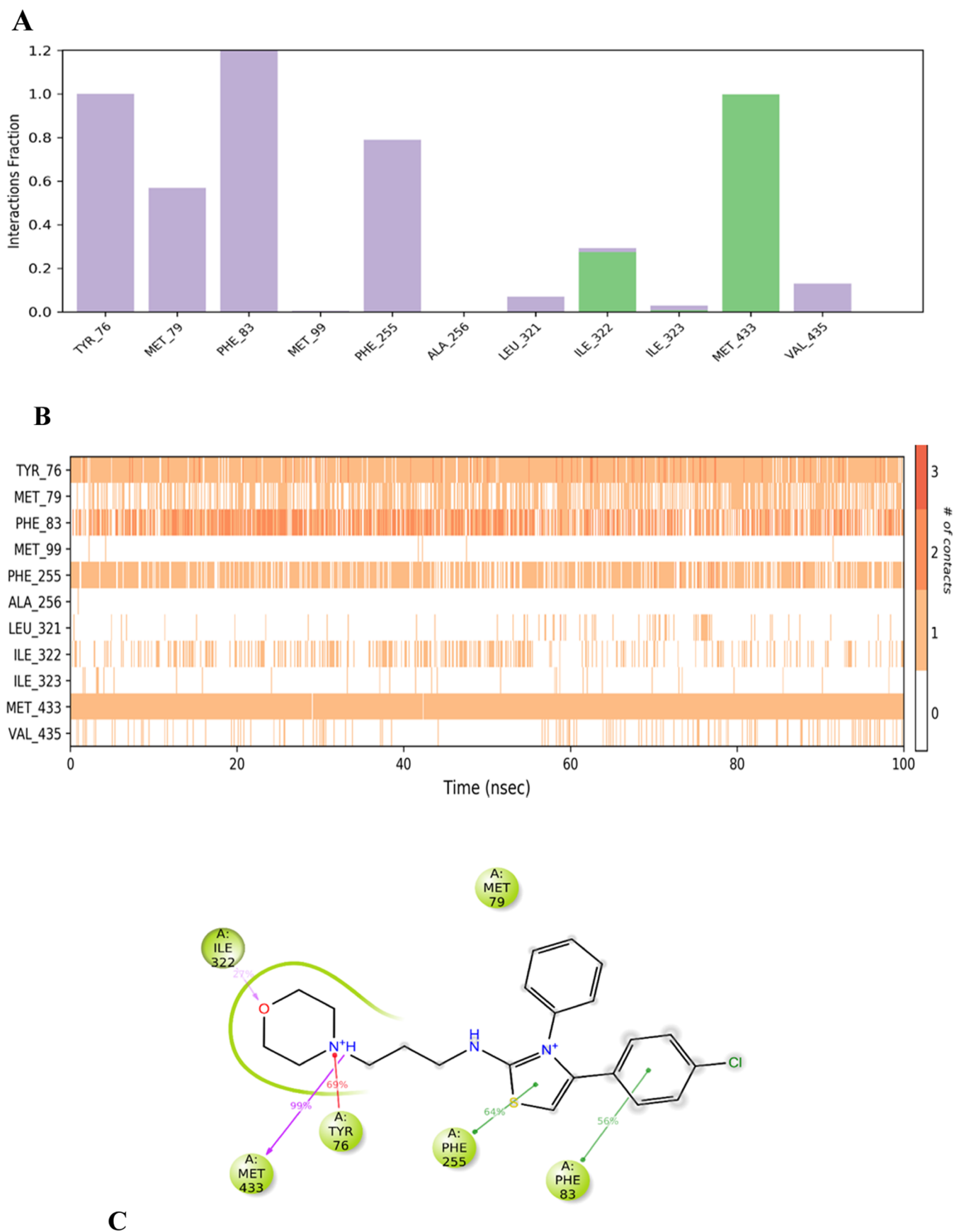
Figure 10. Interactions diagrams of compound **2d**−14α-demethylase enzyme complex. (A) Interaction fractions by residue during the simulation (green: H-bond, purple: hydrophobic interaction). (B) Plot of number of interactions vs residue index. (C) Diagram of the 2D interaction strengths.
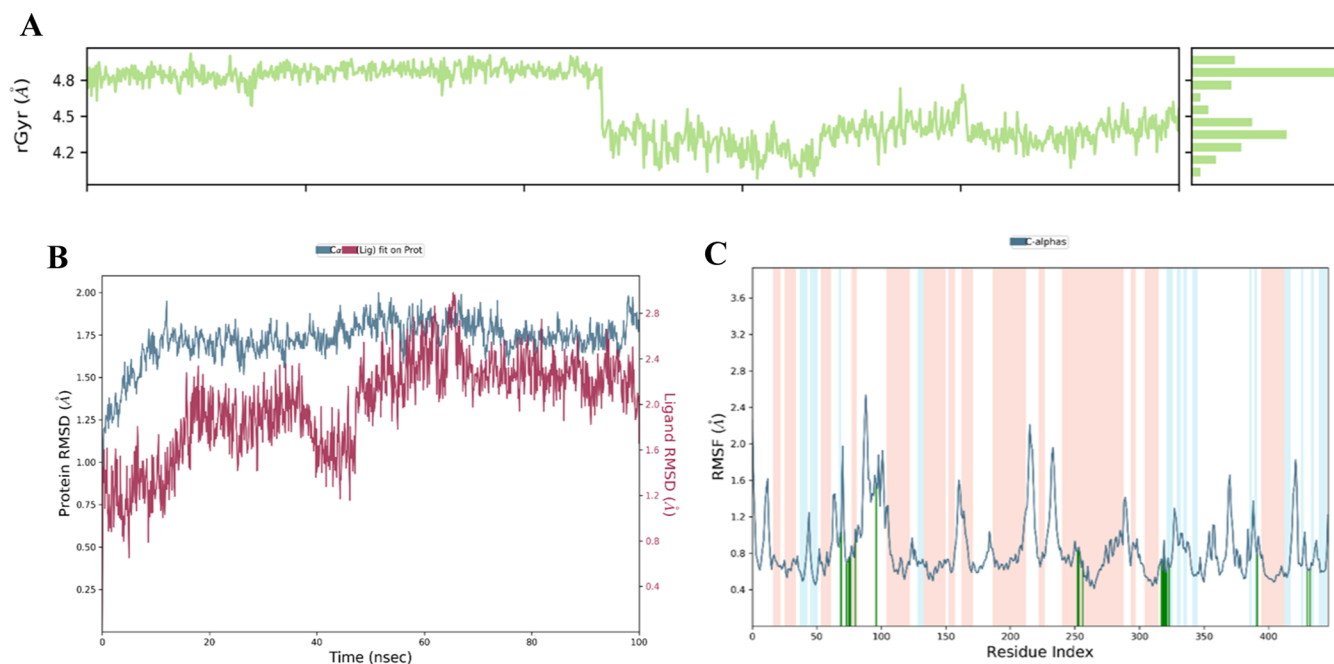
Figure 11. Stability diagrams of compound **2e**−14α-demethylase enzyme complex. (A) Plot of radius of gyration vs time (ns). (B) Plot of RMSD vs time ° (ns). (C) Plot of RMSF vs residue index (The areas were represented in light pink for the helices, light blue for the strands, and white for the loops).

3. CONCLUSIONS

In this study, we designed and synthesized a novel series of morpholine-thiazol hybrid molecules. The compounds underwent thorough spectral analysis followed by an evaluation of their in vitro antifungal activity. Subsequently, ergosterol inhibition was investigated by using GC-MS. The final phase of our work involved an in-depth in silico study.

As a result of the activity studies carried out, compounds **2d** and **2e** showed significant activity against *C. albicans* species (2.47 μM and 2.37 μM/48 h). Active compounds were analyzed for ergosterol biosynthesis inhibition, which is the mechanism of action of azole group antifungals. For this purpose, compounds **2d** and **2e** were incubated for 24 and 48 h at IC$_{50}$ concentrations against *C. parapsilosis*. At the end of the period, it was extracted from the fungal medium, and the amount of ergosterol was determined by GC-MS. As a result of comparisons made with the control group, it was determined that compounds **2d** and **2e** showed activity by inhibiting ergosterol synthesis. Since the pathway of ergosterol synthesis inhibition is based on the inhibition of 14α-demethylase enzyme, which converts lanosterol into ergosterol, in silico studies were carried out using the crystal of this enzyme. The molecular docking studies showed that the thiazole ring of selected derivatives **2d** and **2e** bound to the HEM group of the 14α-demethylase enzyme. It is once again understood that this ring is important for activity. Dynamic studies also show that the compounds remain stable in the enzyme active site for 100 ns and have a high binding potential.

As a result, it is seen that compounds **2d** and **2e** obtained in this study show their antifungal effects by inhibiting ergosterol synthesis. The compounds exhibited their inhibitory potential on the 14α-demethylase enzyme, which converts lanosterol to ergosterol, through their interactions with HEM. This information is promising and forms the basis for future studies.

4. MATERIALS AND METHODS

4.1. Chemistry. *4.1.1. General.* All chemicals were obtained from industrial vendors and used without additional purification. Melting points (mp) were calculated using the uncorrected Mettler Toledo-MP90 Melting Point System. The instruments employed were a ^{13}C NMR Bruker DPX 75 MHz spectrometer and a ^{1}H NMR Bruker DPX 300 FT-NMR (both from Bruker Bioscience, Billerica, MA). 600 μL of DMSO-d6 was used to dissolve a total of 10 mg of the substance. The NMR technique was completed in this manner. On an LCMS-IT-TOF (Shimadzu, Kyoto, Japan) using ESI, mass spectra were obtained. 1500 μL of MeOH was used to dissolve a total of 10 mg of the chemical. The HRMS technique was carried out in this manner.

4.1.2. Synthesis of 1-(3-Morpholinopropyl)-3-phenyl-thiourea. 3-Morpholinopropan-1-aminium (0.0693 mol) was refluxed with phenyl isothiocyanate (0.0693 mol) in ethanol (50 mL) for 6 h. At the end of the reaction, ethanol was evaporated and the precipitated product was purified via recrystallization to obtain 1-(3-morpholinopropyl)-3-phenyl-thiourea.

4.1.3. Synthesis of N-(3-Morpholinopropyl)-4-(R-phenyl)-3-phenylthiazol-2(3H)-imine Derivatives. From molecule **1** (1-(3-morpholinopropyl)-3-phenylthiourea), 0.00107 mol of bromoacetophenone derivatives was refluxed for 4−8 h. After the reaction was complete, the mixture was cooled to 0 °C to obtain the pure product of **2a**−**2j**.

4.1.3.1. N-(3-Morpholinopropyl)-3-phenyl-4-(p-tolyl)-thiazol-2(3H)-imine (2a). Yield: 75%, M.P.: 179−182 °C. ^{1}H NMR (300 MHz, DMSO-d_6): δ = 1.99 (2H,s, propyline-H), 2.37(3H, s, CH$_3$), 3.06 (2H, s, morpholinopropyl-H), 3.35−3.44 (4H, m, morpholin-H), 3.77−3.81 (6H, m, morpholinopropyl-H), 6.20 (1H, s, thiazol-1H), 7.02−7.04 (3H, m, Ar−H). 7.31−7.40 (6H, m, Ar−H). ^{13}C NMR (75 MHz, DMSO-d_6): δ = 22.22, 23.89, 51.36, 53.30, 53.70, 63.79,
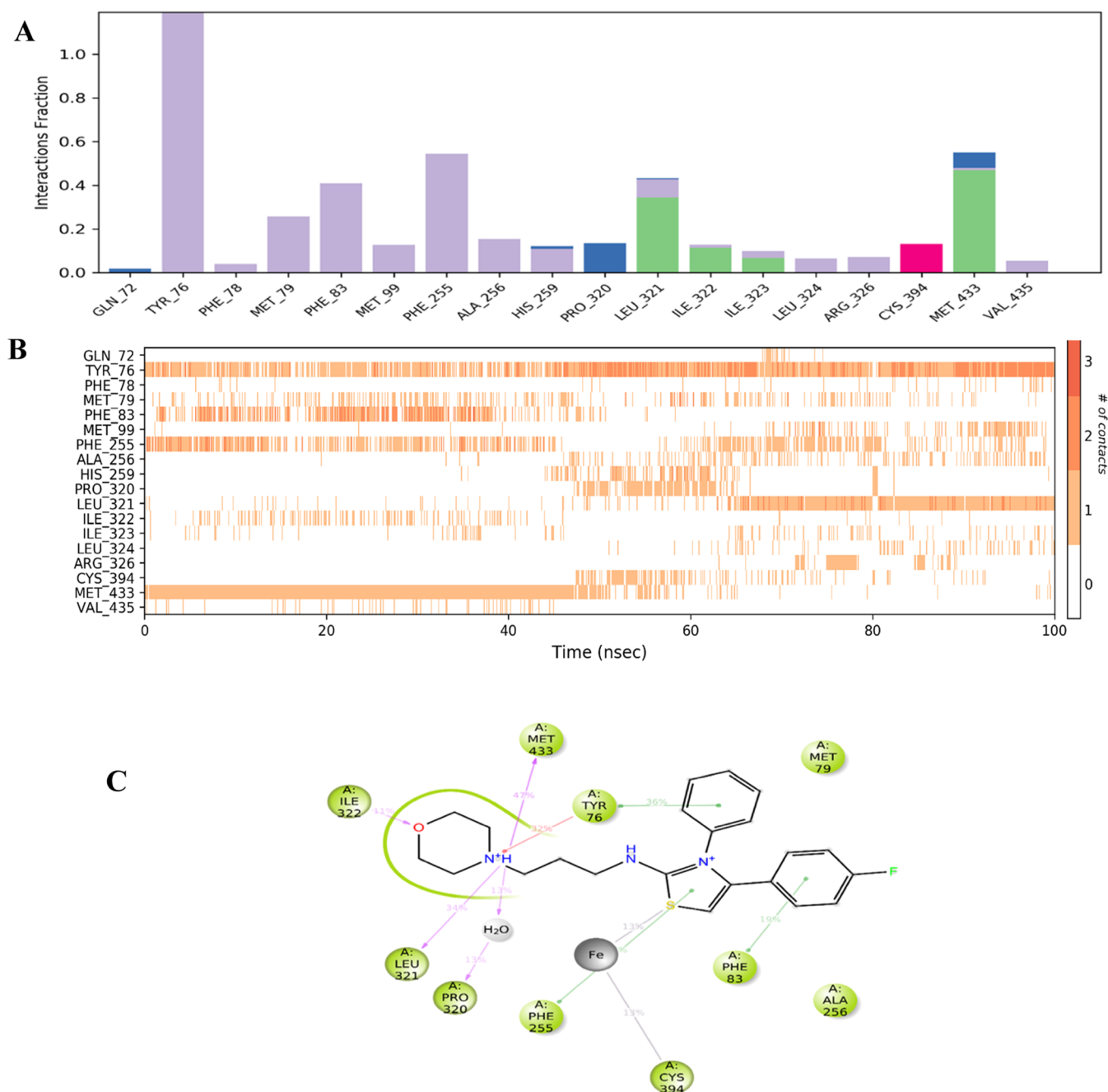
Figure 12. Plots of the MDS results for the compound **2e**−14α-demethylase enzyme complex. Stability properties: (A) interaction fractions by residue during the simulation (green: H-bond, purple: hydrophobic interaction). (B) Plot of number of interactions vs residue index; (C) diagram of the 2D interaction strengths.

97.98, 120.68, 122.79, 124.59, 128.38,128.90, 128.98, 130.51, 130.99, 131.10, 139.53. HRMS (m/z): [M + H]$^+$ calcd for $C_{23}H_{27}N_3OS$ [M + H]$^+$: 394.1948; found: 394.1938.

4.1.3.2. N-(3-Morpholinopropyl)-4-(4-nitrophenyl)-3-phenylthiazol-2(3H)-imine (2b). Yield: 80%, M.P.: 123−125 °C. ^{1}H NMR (300 MHz, DMSO-d_6): δ = 2.09−2.24 (6H, m, −3CH$_2$, morpholinopropyl-H), 2.97−3.23 (2H, m, propyline-H), 3.41−3.55 (6H, m, morpholinopropyl-H), 6.83−6.90 (1H, m, thiazol-1H), 6.92−7.04, (2H, m, Ar -H), 7.19−7.36 (2H, m, Ar−H), 7.55 (1H, s, Ar -H), 7.75−7.91 (2H, d, J = 8.9 Hz, Ar−H), 8.22−8.38 (2H, d, $J_=$ 8.9, Ar−H). ^{13}C NMR (75 MHz, DMSO-d_6): δ = 24.31, 42.15, 42.92, 53.32, 55.98, 66.41, 93.37, 122.18, 123.25, 124.02, 128.39, 129.34, 147.79, 150.50, 151.71,

156.98. HRMS (m/z): [M + H]$^+$ calcd for $C_{22}H_{24}N_4O_3S$: 425.1642; found: 425.1650.

4.1.3.3. 4-(4-Methoxyphenyl)-N-(3-morpholinopropyl)-3-phenylthiazol-2(3H)-imine (2c). Yield: 78%, M.P: 155−159 °C. ^{1}H NMR (300 MHz, DMSO-d_6): δ = 1.94−1.96 (2H, br.s, propyline-H), 2.78−2.94 (6H, m, morpholinopropyl-H), 3.62−3.69 (6H, m, morpholinopropyl-H), 3.80 (3H, s, O−CH$_3$), 6.19 (1H, s, thiazol-1H), 6.98−7.19 (5H, m, Ar-H), 7.29−7.41 (2H, m, Ar -H), 7.46−7.56 (2H, d, $J_=$ 8.72 Hz, Ar -H).^{13}C NMR (75 MHz, DMSO-d_6): δ = 23.23, 42.78, 51.99, 54.36, 55.79, 64.73, 96.0, 114.67, 121.64, 123.20, 123.60, 129.95, 130.95, 139.07, 151.65,159.41,160.33. HRMS (m/z):
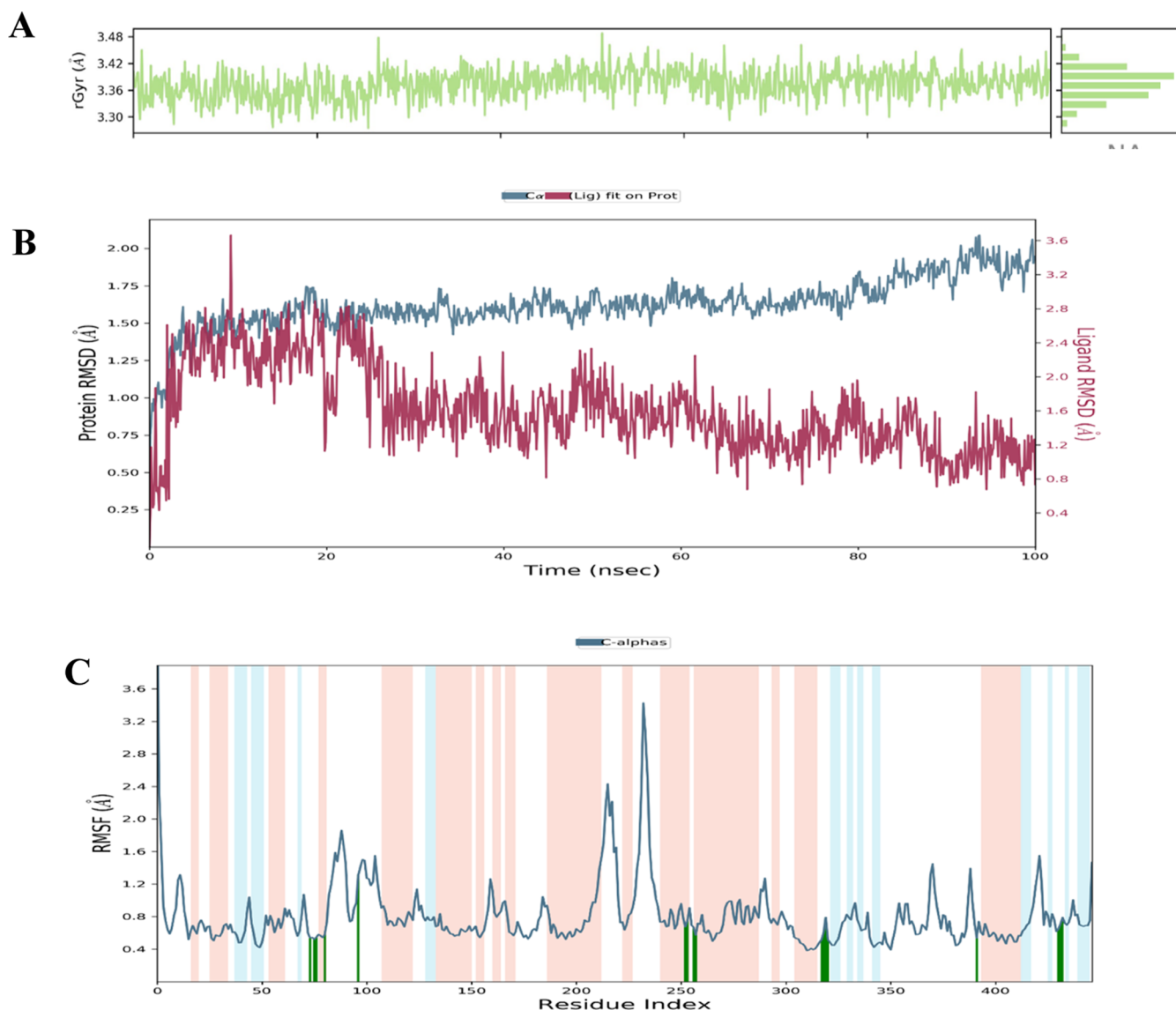
Figure 13. Stability diagrams of fluconazole−14α-demethylase enzyme complex. (A) Plot of radius of gyration vs time (ns). (B) Plot of RMSD vs time ° (ns). (C) Plot of RMSF vs residue index. (The areas were represented in light pink for the helices, light blue for the strands, and white for the loops).

$[M + H]^+$ calcd for C_{23} $H_{27}N_3O_2S$: 410.1897; found: 410.1908.

4.1.3.4. 4-(4-Chlorophenyl)-N-(3-morpholinopropyl)-3-phenylthiazol-2(3H)-imine (2d). Yield: 77%, M.P.: 200−204 °C. ^{1}H NMR (300 MHz, DMSO-d_6): δ = 1.99 (2H, br.s., propyline-H), 3.06−3.44 (10H, m, morpholinopropyl-H), 3.72−3.77 (2H, m, morpholinopropyl-H), 6.30 (1H,s, thiazol-1H), 6.95−7.11 (3H, m, Ar−H), 7.32−7.37 (2H, m, Ar−H), 7.4−7.6 (4H, m, Ar-H). ^{13}C NMR (75 MHz, DMSO-d_6): δ = 22.65, 42.64, 51.39, 53.70, 63.75, 97.70, 121.64, 123.43, 129.47, 130.01, 130.14, 131.37, 134.63, 138.55, 151.48,159.43. HRMS (m/z): $[M + H]^+$ calcd for C_{22} H_{24} N_3OSCl: 414.1401; found: 414.1419.

4.1.3.5. 4-(4-Fluorophenyl)-N-(3-morpholinopropyl)-3-phenylthiazol-2(3H)-imine (2e). Yield: 72%, M.P: 190−193 °C. ^{1}H NMR (300 MHz, DMSO-d_6): δ = 2.00−2.05(2H, br.s, propyline-H) 3.02−3.19 (10H, m, morpholinopropyl-H), 3.38−3.46 (2H, m, morpholinopropyl-H), 6.34 (1H, s, thiazol-1H), 7.08−7.10 (2H, d, J = 6.09 Hz, Ar -H), 7.30−7.44 (5H, m, Ar-H), 7.50−7.65 (2H, m, Ar-H), ^{13}C NMR (75

MHz, DMSO-d_6): δ = 22.47, 42.73, 51.31, 53.53, 63.66, 97.24, 116.33, 116.62, 122.09, 124.00, 127.45, 129.28, 130.09, 132.17, 138.92,161.47, 164.74. HRMS (m/z): $[M + H]^+$ calcd for C_{22} $H_{24}N_3OFS$: 398.1697; found: 398.1708.

4.1.3.6. 4-(2-((3-Morpholinopropyl)imino)-3-phenyl-2,3-dihydrothiazol-4-yl)benzonitrile (2f). Yield: 70%, M.P.: 126−128 °C. ^{1}H NMR (300 MHz, DMSO-d_6): δ = 1.83−2.33 (6H, m, morpholinopropyl-H), 381−3.97 (8H, m, morpholinopropyl-H), 6.46 (1H, s, thiazol-1H) 6.98−7.00 (1H, m, Ar−H), 7.04−7.11(2H, m, Ar-H), 7.33−7.46 (2H, m, Ar-H), 7.70−7.86 (2H, d, J = 8.04 Hz, Ar-H), 7.97−8.14 (2H, d, J=8.17 Hz, Ar-H). ^{13}C NMR (75 MHz, DMSO-d_6): δ = 23.68, 43.24, 52.96, 54.74, 65.65, 98.92, 112.19, 118.90, 121.22, 121.48, 122.38, 123.34, 129.17, 130.02, 130.13, 133.23, 136.06, 138.45, 151.59, 159.18. HRMS (m/z): $[M + H]^+$ calcd for C_{23} H_{24} N_4OS: 405.1744; found: 405.1755.

4.1.3.7. 4-([1,1′-Biphenyl]-4-yl)-N-(3-morpholinopropyl)-3-phenylthiazol-2(3H)-imine (2g). Yield: 65%, M.P.: 184−189 °C. ^{1}H NMR (300 MHz, DMSO-d_6): δ = 2.05 (2H, br.s, (propyline-H) 3.37−3.46 (4H, m, morpholinopropyl-H),
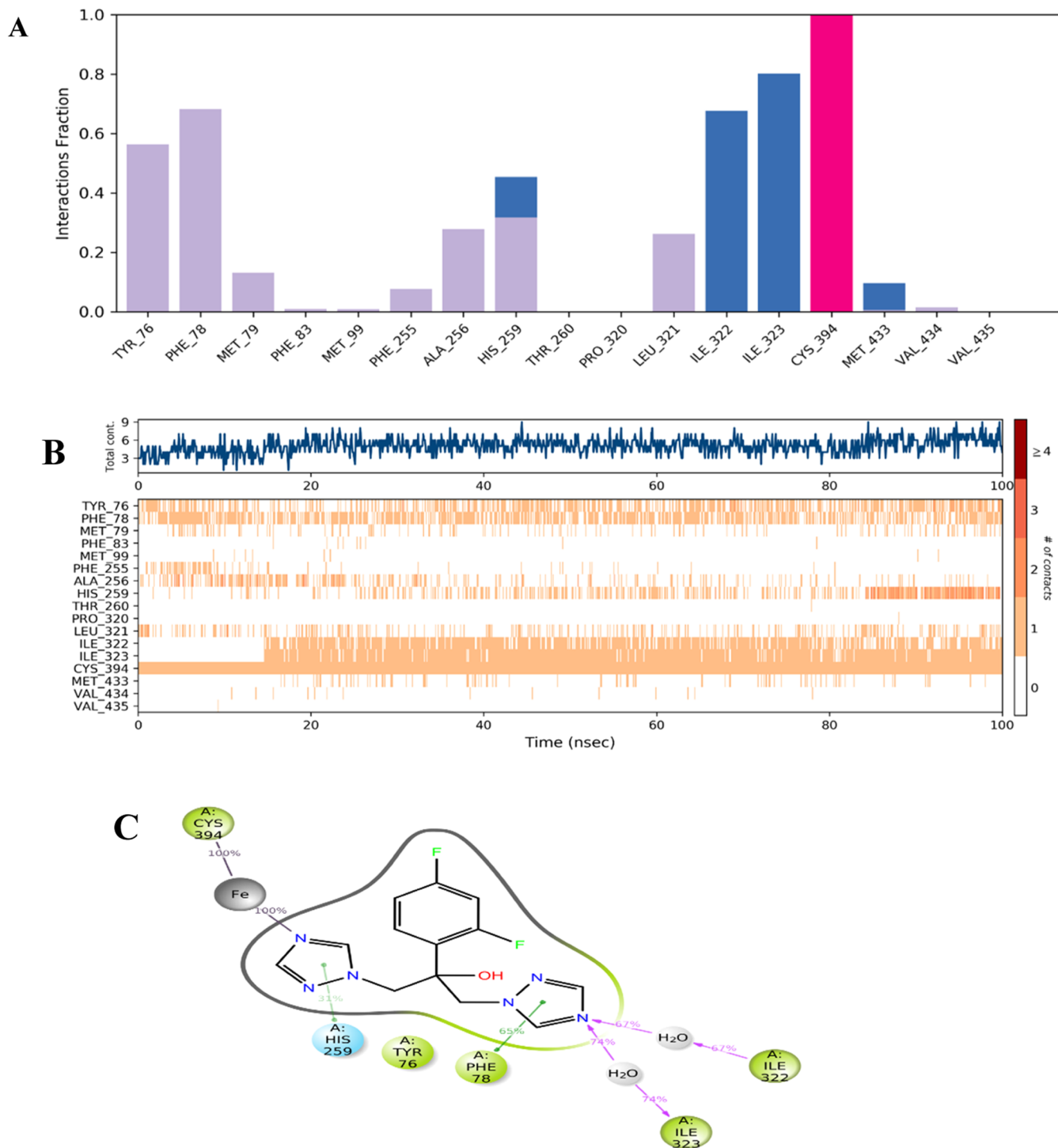
Figure 14. Plots of the MDS results for the compound fluconazole−14α-demethylase enzyme complex. Stability properties: (A) Interaction fractions by residue during the simulation (blue: H-bond, purple: hydrophobic interaction; pink: π−π stuck). (B) Plot of number of interactions vs residue index; (C) Diagram of the 2D interaction strengths.

3.84−3.93 (8H, m, morpholinopropyl-H), 6.31 (1H, s, thiazol-1H), 6.98−7.14 (3H, m, Ar−H), 7.26−7.91 (11H m, biphenyl-H). ^{13}C NMR (75 MHz, DMSO-d_6): δ = 22.70, 42.74, 51.39, 53.76, 63.77, 97.30, 121.71, 123.43, 127.20, 127.58, 128.47, 129.60, 130.02, 130.34, 139.50, 139.57, 141.36, 151.52,159.65. HRMS (m/z): [M + H]$^+$ calcd for $C_{28}H_{29}N_3OS$: 456.2104; found: 456.2110.

4.1.3.8. 4-(2,4-Dichlorophenyl)-N-(3-morpholinopropyl)-3-phenylthiazol-2(3H)-imine (2h). Yield: 68%, M.P.: 103−105 °C. ^{1}H NMR (300 MHz, DMSO-d_6): δ = 1.64−1.69 (2H,br.s, propyline-H), 2.08−2.16 (8H, m, morpholinopropyl-H), 3.79 (4H, br.s, morpholinopropyl-H), 6.30 (1H, s, thiazol-1H), 6.90−7.07 (4H, m, Ar−H), 7.23−7.41 (3H, m, Ar-H), 7.53−7.68 (3H, m, Ar−H), 7.88 (1H, s, Ar -H). ^{13}C NMR (75 MHz, DMSO-d_6): δ = 24.12, 43.11, 53.26, 55.19, 66.44, 98.01,

121.46, 123.12, 128.31, 129.56, 129.73, 129.95, 134.43, 135.22, 135.95, 151.63,158.03. HRMS (m/z): $[M + H]^+$ calcd for $C_{22}H_{23}N_3OSCl_2$ $[M + H]+$ 448.1012; found: 448.1015.

4.1.3.9. 4-(2,4-Difluorophenyl)-N-(3-morpholinopropyl)-3-phenylthiazol-2(3H)-imine (2i). Yield: 84%, M.P: 209−211 °C. ^1H NMR (300 MHz, DMSO-d_6): δ = 1.99 (2H, br.s., (propyline-H) 2.99−3.13 (4H, m, morpholinopropyl-H), 3.60−3.81 (8H, m, morpholinopropyl-H), 6.37 (1H, s, thiazol-1H), 6.97−7.12(3H, m, Ar-H), 7.23−7.43 (3H, m, Ar−H), 7.46−7.56 (1H, m, Ar−H), 7.63−7.74 (1H, m, Ar-H). ^{13}C NMR (75 MHz, DMSO-d_6): δ = 22.27, 42.47, 51.17, 53.56, 63.57, 99.23, 105.33, 112.79, 115.33, 121.62, 123.41, 129.98, 132.25, 134.26, 151.49, 158.70, 162.17, 165.48. HRMS (m/z): $[M + H]^+$ calcd for $C_{22}H_{23}N_3OF_2S$:416.1603; found: 416.1616.

4.1.3.10. 4-(2,4-Dimethylphenyl)-N-(3-morpholinopropyl)-3-phenylthiazol-2(3H)-imine (2j). Yield: 75%, M.P.: 67−69 °C. ^1H NMR (300 MHz, DMSO-d_6): δ = 1.65 (2H, br.s, propyline-H) 1.90−2.10 (4H, m, morpholinopropyl-H), 2.17 (3H, s, methyl-H), 2.32 (3H, s, methyl-H), 2.24−2.26 (2H, d, J = 5.47 Hz, morpholinopropyl-H), 2.39(1H, s, propyline-H), 3.39−3.79 (4H, br.s, morpholinopropyl-H), 6.08 (1H, s, thiazol-1H), 6.93−7.12(4H, m, Ar-H), 7.16−7.25 (2H, m, Ar-H), 7.27−7.38 (2H, m, Ar-H). ^{13}C NMR (75 MHz, DMSO-d_6): δ = 19.73, 19.76, 21.25, 42.75, 53.00, 55.13, 66.26, 95.69, 121.55, 122.95, 127.05, 129.42, 129.88, 130.88, 131.28, 137.61,138.43, 139.56, 151.71, 158.51. HRMS (m/z): $[M + H]^+$ calcd for $C_{24}H_{29}N_3OS$: 408.2104; found: 408.2113.

4.2. In Vitro Antifungal Activity. In vitro antifungal activity for compounds **2a-2j** was determined fluorimetrically according to the EUCAST method, as previously reported by our team.[27,41−45] The antifungal activity results are listed in Table 3.

4.3. Analysis of Ergosterol Synthesis Inhibition. The detection of ergosterol levels of the selected compounds was carried out according to a previous report.[46] The experimental procedure was as previously reported.[45]

4.4. Cytotoxicity Analysis. Cytotoxicity tests were performed as previously reported using NIH3T3 cells by the MTT method.[47−50]

4.5. Prediction of ADME Parameters. To evaluate the drug-likeness properties of the synthesized compounds **2a−2j**, ADME predictions were performed using SwissADME[34] ChemDraw 17.0.[35] As mentioned in Table 5, the results of the ADME screening reveal multiple descriptors belonging to different properties such as physicochemical qualities, lipophilicity, water solubility, pharmacokinetics, drug-likeness, and medicinal chemistry. GI absorption and P-glycoprotein reflected the absorption properties of a compound.

4.6. Molecular Docking Studies. The binding mechanisms of substances **2d** and **2e** to the active site of the 14α-demethylase enzyme were determined by using a structure-based in silico technique. From the Protein Data Bank website (www.pdb.org), the crystal structure of 14α-demethylase enzyme (PDB ID: 1EA1) was obtained. Utilizing the Schrödinger Maestro[51] interface, docking studies were carried out using Schrödinger program interfaces with standard docking procedure.[52−54]

4.7. Molecular Dynamic Studies. 100 ns molecular dynamics studies were performed using the POPE membrane model as previously described using the Maestro Desmond interface.[55−57]

■ AUTHOR INFORMATION

Corresponding Author

Derya Osmaniye − *Department of Pharmaceutical Chemistry, Faculty of Pharmacy and Central Research Laboratory, Faculty of Pharmacy, Anadolu University, Eskişehir 26470, Turkey;* ⓞ orcid.org/0000-0002-0499-436X; Email: dosmaniye@anadolu.edu.tr

Authors

Sazan Haji Ali − *Department of Pharmaceutical Chemistry, Faculty of Pharmacy, Hawler Medical University, Erbil 44000, Iraq; Graduate Education Institute, Anadolu University, Eskişehir 26470, Turkey*

Begüm Nurpelin Sağlık − *Department of Pharmaceutical Chemistry, Faculty of Pharmacy and Central Research Laboratory, Faculty of Pharmacy, Anadolu University, Eskişehir 26470, Turkey;* ⓞ orcid.org/0000-0002-0151-6266

Serkan Levent − *Department of Pharmaceutical Chemistry, Faculty of Pharmacy and Central Research Laboratory, Faculty of Pharmacy, Anadolu University, Eskişehir 26470, Turkey*

Yusuf Özkay − *Department of Pharmaceutical Chemistry, Faculty of Pharmacy and Central Research Laboratory, Faculty of Pharmacy, Anadolu University, Eskişehir 26470, Turkey*

Zafer Asım Kaplancıklı − *Department of Pharmaceutical Chemistry, Faculty of Pharmacy, Anadolu University, Eskişehir 26470, Turkey*

Complete contact information is available at:
https://pubs.acs.org/10.1021/acsomega.3c07879

Notes

The authors declare no competing financial interest.

■ REFERENCES

(1) WHO fungal priority pathogens list to guide research, development and public health action. https://www.who.int/publications-detail-redirect/9789240060241 (accessed April 22, 2023).

(2) Güzel, E.; Acar Çevik, U.; Evren, A. E.; Bostancı, H. E.; Gül, Ü. D.; Kayış, U.; Özkay, Y.; Kaplancıklı, Z. A. Synthesis of Benzimidazole-1,2,4-Triazole Derivatives as Potential Antifungal Agents Targeting 14α-Demethylase. *ACS Omega* **2023**, *8* (4), 4369−4384.

(3) Tudela, J. L. R.; Denning, D. W. Recovery from Serious Fungal Infections Should Be Realisable for Everyone. *Lancet Infect. Dis.* **2017**, *17* (11), 1111−1113.

(4) Hilmioğlu-Polat, S.; Seyedmousavi, S.; Ilkit, M.; Hedayati, M. T.; Inci, R.; Tumbay, E.; Denning, D. W. Estimated Burden of Serious Human Fungal Diseases in Turkey. *Mycoses* **2019**, *62* (1), 22−31.

(5) Hosseini-Moghaddam, S. M.; Ouédraogo, A.; Naylor, K. L.; Bota, S. E.; Husain, S.; Nash, D. M.; Paterson, J. M. Incidence and Outcomes of Invasive Fungal Infection among Solid Organ Transplant Recipients: A Population-Based Cohort Study. *Transplant Infect. Dis.* **2020**, *22* (2), No. e13250.

(6) Fuentefria, A. M.; Pippi, B.; Lana, D. F. D.; Donato, K. K.; de Andrade, S. F. Antifungals Discovery: An Insight into New Strategies to Combat Antifungal Resistance. *Lett. Appl. Microbiol.* **2018**, *66* (1), 2−13, DOI: 10.1111/lam.12820.

(7) Jabli, S.; Hrichi, S.; Chaabane-Banaoues, R.; Molton, F.; Loiseau, F.; Roisnel, T.; Turowska-Tyrk, I.; Babba, H.; Nasri, H. Study on the Synthesis, Physicochemical, Electrochemical Properties, Molecular Structure and Antifungal Activities of the 4-Pyrrolidinopyridine Mg(II) Meso-Tetratolylporphyrin Complex. *J. Mol. Struct.* **2022**, *1261*, No. 132882.

(8) Waseem, M.; Thakur, J. K.; Subbarao, N. Prediction of Novel and Potent Inhibitors of Lanosterol 14-α Demethylase. *J. Biomol. Struct. Dyn.* **2023**, *41* (12), 5744−5756.

(9) Rossatto, F. C. P.; Tharmalingam, N.; Escobar, I. E.; d'Azevedo, P. A.; Zimmer, K. R.; Mylonakis, E. Antifungal Activity of the Phenolic Compounds Ellagic Acid (EA) and Caffeic Acid Phenethyl Ester (CAPE) against Drug-Resistant Candida Auris. *J. Fungi* **2021**, *7* (9), 763 DOI: 10.3390/jof7090763.

(10) Chiurlo, M.; Mastrangelo, A.; Ripa, M.; Scarpellini, P. Invasive Fungal Infections in Patients with COVID-19: A Review on Pathogenesis, Epidemiology, Clinical Features, Treatment, and Outcomes. *New Microbiol.* **2021**, *44*, 71−83.

(11) Raut, A.; Huy, N. T. Rising Incidence of Mucormycosis in Patients with COVID-19: Another Challenge for India amidst the Second Wave? *Lancet Respir. Med.* **2021**, *9* (8), No. e77.

(12) Statistics | Invasive Candidiasis | Candidiasis | Types of Diseases | Fungal Diseases | CDC. https://www.cdc.gov/fungal/diseases/candidiasis/invasive/statistics.html (accessed April 22, 2023).

(13) Cleveland, A. A.; Harrison, L. H.; Farley, M. M.; Hollick, R.; Stein, B.; Chiller, T. M.; Lockhart, S. R.; Park, B. J. Declining Incidence of Candidemia and the Shifting Epidemiology of *Candida* Resistance in Two US Metropolitan Areas, 2008−2013: Results from Population-Based Surveillance. *PLoS One* **2015**, *10* (3), No. e0120452.

(14) Van Daele, R.; Spriet, I.; Wauters, J.; Maertens, J.; Mercier, T.; Van Hecke, S.; Brüggemann, R. Antifungal Drugs: What Brings the Future? *Med. Mycol.* **2019**, *57* (Supplement_3), S328−S343.

(15) Liu, W.; Sun, Z.; An, Y.; Liu, Y.; Fan, H.; Han, J.; Sun, B. Construction and Activity Evaluation of Novel Dual-Target (SE/CYP51) Anti-Fungal Agents Containing Amide Naphthyl Structure. *Eur. J. Med. Chem.* **2022**, *228*, No. 113972.

(16) Bhattacharya, S.; Sae-Tia, S.; Fries, B. C. Candidiasis and Mechanisms of Antifungal Resistance. *Antibiotics* **2020**, *9* (6), 312.

(17) Chatelon, J.; Cortegiani, A.; Hammad, E.; Cassir, N.; Leone, M. Choosing the Right Antifungal Agent in ICU Patients. *Adv. Ther.* **2019**, *36* (12), 3308−3320.

(18) Emami, S.; Tavangar, P.; Keighobadi, M. An Overview of Azoles Targeting Sterol 14α-Demethylase for Antileishmanial Therapy. *Eur. J. Med. Chem.* **2017**, *135*, 241−259.

(19) Warrilow, A. G.; Parker, J. E.; Kelly, D. E.; Kelly, S. L. Azole Affinity of Sterol 14α-Demethylase (CYP51) Enzymes from *Candida albicans* and *Homo sapiens*. *Antimicrob. Agents Chemother.* **2013**, *57* (3), 1352−1360.

(20) Lupetti, A.; Danesi, R.; Campa, M.; Del Tacca, M.; Kelly, S. Molecular Basis of Resistance to Azole Antifungals. *Trends Mol. Med.* **2002**, *8* (2), 76−81.

(21) Yang, L. Design, Synthesis, and Antifungal Activity of Novel Benzimidazole Derivatives Bearing Thioether and Carbamate Moieties. *J. Chem.* **2022**, *2022*, No. e8646557.

(22) Obydennov, K. L.; Kalinina, T. A.; Galieva, N. A.; Beryozkina, T. V.; Zhang, Y.; Fan, Z.; Glukhareva, T. V.; Bakulev, V. A. Synthesis, Fungicidal Activity, and Molecular Docking of 2-Acylamino and 2-Thioacylamino Derivatives of 1*H*-Benzo[*d*]Imidazoles as Anti-Tubulin Agents. *J. Agric. Food Chem.* **2021**, *69* (40), 12048−12062.

(23) Marzi, M.; Farjam, M.; Kazeminejad, Z.; Shiroudi, A.; Kouhpayeh, A.; Zarenezhad, E. A Recent Overview of 1,2,3-Triazole-Containing Hybrids as Novel Antifungal Agents: Focusing on Synthesis, Mechanism of Action, and Structure-Activity Relationship (SAR). *J. Chem.* **2022**, *2022*, No. e7884316.

(24) Teixeira, M. M.; Carvalho, D. T.; Sousa, E.; Pinto, E. New Antifungal Agents with Azole Moieties. *Pharmaceuticals* **2022**, *15* (11), 1427.

(25) Lino, C. I.; de Souza, I. G.; Borelli, B. M.; Matos, T. T. S.; Teixeira, I. N. S.; Ramos, J. P.; de Souza Fagundes, E. M.; de Oliveira Fernandes, P.; Maltarollo, V. G.; Johann, S.; de Oliveira, R. B. Synthesis, Molecular Modeling Studies and Evaluation of Antifungal Activity of a Novel Series of Thiazole Derivatives. *Eur. J. Med. Chem.* **2018**, *151*, 248−260, DOI: 10.1016/j.ejmech.2018.03.083.

(26) Chimenti, F.; Bizzarri, B.; Bolasco, A.; Secci, D.; Chimenti, P.; Granese, A.; Carradori, S.; D'Ascenzio, M.; Lilli, D.; Rivanera, D. Synthesis and Biological Evaluation of Novel 2,4-Disubstituted-1,3-Thiazoles as Anti-*Candida* Spp. Agents. *Eur. J. Med. Chem.* **2011**, *46* (1), 378−382.

(27) Rodriguez-Tudela, J. L.; Arendrup, M. C.; Barchiesi, F.; Bille, J.; Chryssanthou, E.; Cuenca-Estrella, M.; Dannaoui, E.; Denning, D. W.; Donnelly, J. P.; Dromer, F.; Fegeler, W.; Lass-Flörl, C.; Moore, C.; Richardson, M.; Sandven, P.; Velegraki, A.; Verweij, P. EUCAST Definitive Document EDef 7.1: Method for the Determination of Broth Dilution MICs of Antifungal Agents for Fermentative Yeasts: Subcommittee on Antifungal Susceptibility Testing (AFST) of the ESCMID European Committee for Antimicrobial Susceptibility Testing (EUCAST)*. *Clin. Microbiol. Infect.* **2008**, *14* (4), 398−405.

(28) Auffinger, P.; Hays, F. A.; Westhof, E.; Ho, P. S. Halogen Bonds in Biological Molecules. *Proc. Natl. Acad. Sci. U.S.A.* **2004**, *101* (48), 16789−16794.

(29) PODUNAVAC-KUZMANOVIĆ, S.; MARKOV, S.; BARNA, D. RELATIONSHIP BETWEEN THE LIPOPHILICITY AND ANTIFUNGAL ACTIVITY OF SOME BENZIMIDAZOLE DERIVATIVES. *J. Theor. Comput. Chem.* **2007**, *06* (04), 687−698, DOI: 10.1142/S0219633607003441.

(30) Wu, Z.-Y.; Liu, N.; Qin, B.; Huang, L.; Yu, F.; Qian, K.; Morris-Natschke, S. L.; Jiang, S.; Chen, C. H.; Lee, K.-H.; Xie, L. Optimization of Antiviral Potency and Lipophilicity of Halogenated 2,6-Diarylpyridinamines (DAPAs) as a Novel Class of HIV-1 NNRTIs. *ChemMedChem* **2014**, *9* (7), 1546−1555.

(31) Abe, F.; Usui, K.; Hiraki, T. Fluconazole Modulates Membrane Rigidity, Heterogeneity, and Water Penetration into the Plasma Membrane in *Saccharomyces cerevisiae*. *Biochemistry* **2009**, *48* (36), 8494−8504.

(32) Perfect, J. R. The Antifungal Pipeline: A Reality Check. *Nat. Rev. Drug Discovery* **2017**, *16* (9), 603−616.

(33) Robbins, N.; Wright, G. D.; Cowen, L. E. Antifungal Drugs: The Current Armamentarium and Development of New Agents. *Microbiol. Spectr.* **2016**, *4* (5), 4−5, DOI: 10.1128/microbiolspec.FUNK-0002-2016.

(34) SwissADME. http://www.swissadme.ch/ (accessed February 18, 2023).

(35) *ChemOffice and ChemDraw*; Version 17.0 Released; PerkinElmer. https://informatics-support.perkinelmer.com/hc/en-us/articles/4408274338580-ChemOffice-and-ChemDraw-version-17-0-released (accessed May 11, 2023).

(36) Sharma, P.; Shanavas, A. Natural Derivatives with Dual Binding Potential against SARS-CoV-2 Main Protease and Human ACE2 Possess Low Oral Bioavailability: A Brief Computational Analysis. *J. Biomol. Struct. Dyn.* **2021**, *39*, 5819−5830, DOI: 10.1080/07391102.2020.1794970.

(37) Bank, R. P. D.; RCSB PDB - 1EA1. Cytochrome P450 14 alpha-sterol demethylase CYP51) from *Mycobacterium tuberculosis* in complex with fluconazole. https://www.rcsb.org/structure/1EA1 (accessed May 12, 2023).

(38) Macchiarulo, A.; Costantino, G.; Fringuelli, D.; Vecchiarelli, A.; Schiaffella, F.; Fringuelli, R. 1,4-Benzothiazine and 1,4-Benzoxazine

Imidazole Derivatives with Antifungal Activity: A Docking Study. *Bioorg. Med. Chem.* **2002**, *10* (11), 3415−3423.

(39) Jeschke, P. The Unique Role of Halogen Substituents in the Design of Modern Agrochemicals. *Pest Manage. Sci.* **2010**, *66* (1), 10−27.

(40) *M.-D.I. Tools*, Schrödinger Release 2018-3: Prime, (2018); Schrödinger, LLC: New York, NY, 2020.

(41) Palomino, J.-C.; Martin, A.; Camacho, M.; Guerra, H.; Swings, J.; Portaels, F. Resazurin Microtiter Assay Plate: Simple and Inexpensive Method for Detection of Drug Resistance in *Mycobacterium tuberculosis. Antimicrob. Agents Chemother.* **2002**, *46* (8), 2720−2722.

(42) Kaplancıklı, Z. A.; Levent, S.; Osmaniye, D.; Sağlık, B. N.; Çevik, U. A.; Çavuşoğlu, B. K.; Özkay, Y.; Ilgın, S. Synthesis and Anticandidal Activity Evaluation of New Benzimidazole-Thiazole Derivatives. *Molecules* **2017**, *22* (12), 2051 DOI: 10.3390/molecules22122051.

(43) Osmaniye, D.; Cavusoglu, B. K.; Saglik, B. N.; Levent, S.; Cevik, U. A.; Atli, O.; Ozkay, Y.; Kaplancikli, Z. A. Synthesis and Anticandidal Activity of New Imidazole-Chalcones. *Molecules* **2018**, *23* (4), No. 831, DOI: 10.3390/molecules23040831.

(44) Karaburun, A. Ç.; Çevik, U. A.; Osmaniye, D.; Sağlık, B. N.; Çavuşoğlu, B. A.; Levent, S.; Özkay, Y.; Koparal, A. S.; Behçet, M.; Kaplancıklı, Z. A. Synthesis and Evaluation of New 1,3,4-Thiadiazole Derivatives as Potent Antifungal Agents. *Molecules* **2018**, *23* (12), 3129.

(45) Osmaniye, D.; Levent, S.; Sağlık, B. N.; Görgülü, Ş.; Özkay, Y.; Kaplancıklı, Z. A. Synthesis of novel thiazol-2 (3 H)-imine derivatives as ergosterol biosynthesis inhibitors, and elucidation of their structures using a 2D NMR technique. *N. J. Chem.* **2023**, *47* (37), 17558−17566.

(46) Zhu, T.; Chen, X.; Li, C.; Tu, J.; Liu, N.; Xu, D.; Sheng, C. Lanosterol 14α-Demethylase (CYP51)/Histone Deacetylase (HDAC) Dual Inhibitors for Treatment of *Candida tropicalis* and *Cryptococcus neoformans* Infections. *Eur. J. Med. Chem.* **2021**, *221*, No. 113524.

(47) Berridge, M. V.; Berridge, M. V.; Herst, P. M.; Tan, A. S. Tetrazolium Dyes as Tools in Cell Biology: New Insights into Their Cellular Reduction. *Biotechnol. Annu. Rev.* **2005**, *11*, 127−152, DOI: 10.1016/S1387-2656(05)11004-7.

(48) Osmaniye, D.; Çelikateş, B. K.; Sağlık, B. N.; Levent, S.; Çevik, U. A.; Çavuşoğlu, B. K.; Ilgın, S.; Özkay, Y.; Kaplancıklı, Z. A. Synthesis of Some New Benzoxazole Derivatives and Investigation of Their Anticancer Activities. *Eur. J. Med. Chem.* **2021**, *210*, No. 112979, DOI: 10.1016/j.ejmech.2020.112979.

(49) Osmaniye, D.; Levent, S.; Karaduman, A. B.; Ilgın, S.; Özkay, Y.; Kaplancıklı, Z. A. Synthesis of New Benzothiazole Acylhydrazones as Anticancer Agents. *Mol. Basel Switz.* **2018**, *23* (5), No. E1054.

(50) Osmaniye, D.; Levent, S.; Ardıç, C. M.; Atlı, Ö.; Özkay, Y.; Kaplancıklı, Z. A. Synthesis and Anticancer Activity of Some Novel Benzothiazole-Thiazolidine Derivatives. *Phosphorus Sulfur Silicon Relat. Elem.* **2018**, *193* (4), 249−256.

(51) *Maestro*, Schrödinger Release 2020−3; Schrödinger, LLC: New York, NY, USA, 2020.

(52) *Schrödinger Suite 2020 Update 2*; Schrödinger LLC: New York, NY, USA, 2020.

(53) *L. Schrödinger LigPrep*, Version 3.8; Schrödinger, LLC: New York, NY, USA, 2016.

(54) *L. Schrödinger Glide*, Version 7.1; Schrödinger, LLC: New York, NY, USA, 2016.

(55) *Impact S. LLC; Prime*, New York, NY, 2016, Google Scholar; Schrödinger, LLC: New York, NY, 2020.

(56) Osmaniye, D.; Evren, A. E.; Karaca, Ş.; Özkay, Y.; Kaplancıklı, Z. A. Novel Thiadiazol Derivatives; Design, Synthesis, Biological Activity, Molecular Docking and Molecular Dynamics. *J. Mol. Struct.* **2023**, *1272*, No. 134171.

(57) Sağlık, B. N.; Levent, S.; Osmaniye, D.; Evren, A. E.; Karaduman, A. B.; Ozkay, Y.; Kaplancıklı, Z. A. Design, Synthesis, and In Vitro and In Silico Approaches of Novel Indanone Derivatives as Multifunctional Anti-Alzheimer Agents. *ACS Omega* **2022**, *7* (50), 47378−47404.